Transport and Anisotropic Diffusion Models for Movement in Oriented Habitats

Thomas Hillen and Kevin J. Painter

Abstract A common feature of many living organisms is the ability to move and navigate in heterogeneous environments. While models for spatial spread of populations are often based on the diffusion equation, here we aim to advertise the use of transport models; in particular in cases where data from individual tracking are available. Rather than developing a full general theory of transport models, we focus on the specific case of animal movement in oriented habitats. The orientations can be given by magnetic cues, elevation profiles, food sources, or disturbances such as seismic lines or roads. In this case we are able to present and contrast the three most common scaling limits, (i) the parabolic scaling, (ii) the hyperbolic scaling, and (iii) the moment closure method. We clearly state the underlying assumptions and guide the reader to an understanding of which scaling method is used in what kind of situations. One interesting result is that the macroscopic drift velocity is given by the mean direction of the underlying linear features, and the diffusion is given by the variance-covariance matrix of the underlying oriented habitat. We illustrate our findings with specific applications to wolf movement in habitats with seismic lines.

T. Hillen
Centre for Mathematical Biology, University of Alberta, Edmonton AB T6G2G1, Canada, e-mail: thillen@ualberta.ca, supported by NSERC

K.J. Painter
Heriot-Watt University, Edinburgh, EH14 4AS, UK, e-mail: K.Painter@hw.ac.uk, supported by BBSRC.

Contents

1 Introduction

1.1 Biological Motivation

Successful navigation through a complicated and evolving environment is a fundamental task carried out by an enormous range of organisms. Migration paths can be staggering in their length and intricacy: at the microscopic scale, nematode worms can determine the shortest path through the intricate maze-like structure of the soil to locate plant roots [40] while at the macroscopic scale salmon return from the ocean upstream through bifurcating rivers and streams to spawn at their original birth site [27]. Selecting a path requires the detection, processing and integration of a myriad of cues drawn from the surrounding environment. In many instances the intrinsic orientation of the environment provides a valuable navigational aid. The earth's magnetic field provides one such example: species such as turtles and whales use an inbuilt compass to navigate to breeding or feeding grounds [27], while butterflies and other insects fly up slopes to local peaks in a mate locating strategy known as "hilltopping" [38]. Pigeons [26] and cane toads [6] have been shown to fly or hop in the direction of roads, while caribou and wolves move along the seismic lines cut into forests by oil exploration companies [31]. An aligned environment also plays a fundamental role in the migration of individual cells: many cell types, including immune cells, fibroblasts and certain types of cancer cells migrate in alignment with the fibre network constituting the surrounding extracellular matrix (ECM).

The above examples provide the motivation for the present paper where we focus on mathematical models for movement in oriented habitats and their scaling limits. The aim is to clarify some of the tools of the trade, allowing the reader to adapt the methods to any given specific situation, such as those outlined above. In the case of the present paper we shall use cell movement in collagen tissues to derive the model equations, before demonstrating their adaption to wolf movement on seismic lines and the motion of organisms in a stream. We note that these should be considered illustrative examples rather than indepth studies, although we note that a detailed application to glioma growth will be covered in a forthcoming paper [37].

1.2 Mathematical Modelling

Transport models (often referred to as kinetic models) form a powerful tool in the analysis and modelling of animal and cell movement. Modern experimental methods allow us to track an individual's movement in intricate detail, whether by GPS tracking of mammals [41, 31] or through confocal microscopy of cells in tissues

[14, 13]. The wealth of data generated can be employed to extract precise information on mean travel speeds, velocities, the distribution of turning angles, the "choice" of new velocities amongst others. Within this context the transport model fits naturally, relying on particle speed and turning distributions as key inputs.

Transport models have a long history in continuum mechanics. For example, the theory of dilute gases is entirely based on the kinetic Boltzmann equation of interacting gas particles [8]. Over the last few decades this theory has been transferred to the modelling of living entities, with the obvious advantage of shipping previously developed methodologies with it [34, 35, 19, 9, 39, 4]. However, wholesale removal from the shelf of continuum mechanics is inadvisable: methods must be carefully adjusted to reflect the biological situation.

A highly utilized tool in the study of transport models is a consideration of scaling limits, thus allowing approximation to a reduced (and typically simpler) model such as a diffusion- or drift-dominated partial differential equation. A variety of scaling limits have been considered, found under the general headings of *parabolic limit*, *diffusion limit*, *hyperbolic limit*, *Chapman-Enskog expansions*, *Hilbert expansions*, and *moment closures* ([19, 9, 10, 16]) (with, most likely, many further terminologies dispersed throughout the literature).

In the hope that we can make transport equations more broadly accessible for ecological and cellular processes, in this chapter we explore such systems as a means of modelling migration. We will open the following section with a presentation of the transport equation approach, as well as a specific formulation that incorporates guided movement due to a fixed and oriented environment. This relatively simple model will be used to motivate and illustrate the various scalings. Here, with our attention fixed on ecological applications, we restrict attention to the three most commonly used methods: (i) the parabolic scaling, (ii) the hyperbolic scaling, and (iii) the moment closure. We will not attempt to present the most abstract and general theory, rather we focus on a nontrivial and interesting case which retains enough simplicity to directly apply each of the scaling limits above. In particular, we will attempt to answer the following questions:

- Is there a better method among those three methods?
- How and when do we employ hyperbolic scaling, parabolic scaling or moment closure?
- What are the specific assumptions behind these three methods and how do they differ?
- In which cases do these scalings lead to the same results?

While all methods have been discussed individually, as far as we are aware there has not been a study which directly compares these methods in the ecological context. We find that each of the methods (i), (ii) and (iii) have their own range of applicability and there are situations when one is favourable over the other. As it turns out, the parabolic limit (i) plays a central role, as special cases of (ii) and (iii) both lead back to (i). To illustrate the findings and methodologies in a transparent manner we will explore some simple case studies and consider specific applications, including the

movement of wolves and caribou along seismic lines in Western Canada. Finally, we will provide a brief discussion of the findings.

2 Transport equations

The application of transport equations to biological processes grew from seminal work of the 1980s (see [1, 34]) as an approach for modelling biological movement, whether by cells or organisms. Transport equations typically refer to mathematical models in which the particles of interest are structured by their position in space, time and velocity. Here we will use $p(t,x,v)$ to describe the population density of cells/organisms at time $t \geq 0$, location $x \in \Omega \subset \mathbb{R}^n$ and velocity $v \in V \subset \mathbb{R}^n$. We will generally consider an unbounded spatial domain $\Omega = \mathbb{R}^n$ to avoid specifying boundary conditions and, given that we consider biological movement, the set of possible velocities V is taken to be compact. It is worth noting that this is a key distinction from the kinetic theory of gas molecules, where $V = \mathbb{R}^n$ permits (at least theoretically) individual molecules to acquire infinite momentum. Here we shall typically consider $V = [s_1, s_2] \times \mathbb{S}^{n-1}$, with $0 \leq s_1 \leq s_2 < \infty$.

The time evolution of $p(t,x,v)$ is described by the *transport equation*

$$p_t(t,x,v) + v \cdot \nabla p(t,x,v) = \mathscr{L} p(t,x,v)\,, \tag{1}$$

where the index t denotes the partial time derivative and $\mathscr{L}$ is the *turning operator*: a mathematical representation for modelling the velocity changes of the particles. In many instances $\mathscr{L}$ could be described by a nonlinear interaction operator incorporating changes in velocity due to interactions between individuals. For example, the coherence of a fish school is maintained through an individual altering velocity in response to that of an immediate neighbour, while certain populations of cells migrate as a cohort by forming strong adhesive bonds with their neighbours. Here we will ignore such scenarios, thus allowing us to focus our attention on the simpler case of linear operators $\mathscr{L}$.

Typically, $\mathscr{L}$ is defined via an integral operator representation

$$\mathscr{L}\varphi(v) = -\mu\varphi(v) + \mu \int_V T(x,v,v')\varphi(v')dv'\,, \tag{2}$$

where the first term on the right hand side gives the rate at which particles switch away from velocity v and the second term denotes the switching into velocity v from all other velocities. The parameter μ is the *turning rate*, with $1/\mu$ the *mean run time* between individual turns. The kernel $T(x,v,v')$ denotes the probability density of switching velocity from v' to v, given that a turn occurs at location x. The mathematical properties of T set the stage for much of the theory that follows and, it is certainly possible to set down a general theory for transport equations (see for example [19, 39, 7, 25]). However, the resulting burden of advanced functional analysis would overwhelm the aims of the present paper. Rather, we focus on a simple

yet non-trivial case which allows us to present the scaling methods in a transparent manner. Specifically, we restrict to the case in which the turning operator does not depend on the incoming velocity v':

$$T(x,v,v') = q(x,v)$$

where q satisfies $q \geq 0$. This assumption limits the applicability, since animals as well as cells have a tendency to maintain a particular direction (persistence) such that the incoming and outgoing velocities show a strong correlation. Here we ignore this form of persistence, and we assume that the dominating directional cue is given by the oriented environment. As mentioned already, a general treatment is possible, but it would deter from our purpose to present the theory in a relatively transparent way.

2.1 Movement in an oriented environment

Here we present a dedicated and simple model based on the transport equation (1) with turning operator (2) to describe movement in an oriented environment. We follow the modelling approach developed by [17] and extended in [36] to describe contact-guided movement of cells within a network, for example an extracellular matrix (ECM) predominantly composed of collagen fibres. We motivate the model by briefly describing its derivation in relation to cell movement, as in the above articles, while noting that the model itself is quite general and can easily be adapted to model the movement of organisms in an oriented landscape, as shown in later sections.

The ECM imparts orienteering cues to cells through their tendency to follow fibres, a process known as contact guidance [12, 15]. More generally, contact guidance describes the oriented motility response of cells to anisotropy in the environment, whether it arises from collagen fibres, muscle fibres, neuronal axons, arteries and so forth. Contact guidance is believed to play important roles in tissue development, homeostasis and repair, from patterning of the pectoral fin bud of the teleost embryo [45] to immune cell guidance [43, 44] and fibroblast-mediated tissue repair following injury [15]. Particular interest in contact-guided migration of cells further stems from its influence in directing the pathways of invasive cancer cells [13, 14].

Following the approach in [17] and [36], we represent the oriented structure of the environment by defining a directional distribution $\tilde{q}(x,\theta)$ for $\theta \in \mathbb{S}^{n-1}$, with $\tilde{q} \geq 0$ and $\int_{\mathbb{S}^{n-1}} \tilde{q}(x,\theta)d\theta = 1$. In the case of cell migration, the fibres along which cells migrate do not provide a particular direction to movement (i.e. there is no "up" or "down" a collagen fibre) and in such instances we would assume symmetry $\tilde{q}(x,-\theta) = \tilde{q}(x,\theta)$ for all $\theta \in \mathbb{S}^{n-1}$. For more on distinct forms for the directional distribution, see below.

To model contact-guided migration, we assume that cells choose their new direction according to the given fibre network, hence $q(x,v) \sim \tilde{q}(x,\hat{v})$, where $\hat{v} = v/||v||$

denotes the corresponding unit vector. Note that this assumes that cells only take guidance information from the directional distribution: there is no explicit component for random migration or orientation to chemical signalling cues built directly into the turning operator, although these can be built into the directional distribution as we demonstrate later. Since q is a probability distribution on V, and $\tilde{q}$ a probability distribution on $\mathbb{S}^{n-1}$, we need to scale appropriately:

$$q(x,v) := \frac{\tilde{q}(x,\hat{v})}{\omega}, \quad \text{with} \quad \omega = \int_V \tilde{q}(x,\hat{v})dv = \begin{cases} \frac{1}{n}(s_2^n - s_1^n) & \text{for } s_1 < s_2 \\ s^{n-1} & \text{for } s_1 = s_2 = s. \end{cases}$$

For this choice of turning kernel, equation (2) simplifies to

$$\mathscr{L}\varphi(v) = \mu(q(x,v)\bar{\varphi} - \varphi(v)), \qquad \text{with} \quad \bar{\varphi} := \int_V \varphi(v)dv.$$

We make one final simplification, which is to assume individuals have a fixed speed s, i.e. $V = s\mathbb{S}^{n-1}$. While the extension to $V = [s_1, s_2] \times \mathbb{S}^{n-1}$ is trivial, it introduces some cumbersome integration constants that blur the analytical details.

To summarise, the transport model we study in this paper is given by

$$p_t(t,x,v) + v \cdot \nabla p(t,x,v) = \mu(q(x,v)\bar{p}(t,x) - p(t,x,v)) \tag{3}$$

on $\mathbb{R}^n \times s\mathbb{S}^{n-1}$, where $q(x,v)$ is the direction distribution that represents the external network structure.

It is worth noting that different cell types adopt distinct migration strategies, with correspondingly variable degrees of interaction with the surrounding network. For individually migrating cells the two principle migration strategies are amoeboid and mesenchymal. While the former is characterised by fleeting contact between cells and the ECM, and correspondingly minimal distortion of the network [44], the latter involves extensive structural modification of the ECM via a processes of cell-mediated proteolytic degradation. Consequently the stand-alone equation (3) is more appropriately a model for amoeboid rather than mesenchymal migration. The latter would require augmentation of (3) with an evolution equation for varying $q(t,x,v)$ due to cell-matrix interactions: while such extensions have been extensively considered in detail in [17] and [36], we do not consider this further here.

As mentioned earlier, while originally developed in the context of cell migration the above transport equation can easily be adapted to ecological applications. For example, to model the population movements of hilltopping butterflies we would reinterpret p as the density of butterflies, q as a spatially varying directional distribution with a maximum corresponding to the local direction of increasing slope, with parameters s and μ for butterfly speed and frequency of turns to be estimated from tracking of individual flights.

2.2 Environmental distributions

Representing anisotropy of the environment through the directional distribution q provides the means to describe a wide range of oriented landscapes. Here we briefly consider some potential forms for q.

Strictly-aligned environments
A strictly aligned environment with local direction $\gamma \in \mathbb{S}^{n-1}$ can be modelled by choosing the singular q-distribution:

$$q(x,v) = \frac{1}{\omega}\delta_0(\hat{v}-\gamma).$$

The above effectively forces an individual to choose γ as a movement direction following a turn. A full mathematical solution theory of (3) for such q requires a notion of measure valued solutions, which was developed in [18] . We discuss this case in connection to applications in Section 7.3.

Regularly-aligned environments
For many landscapes, while oriented structures provide a directional cue, the individuals will typically move over a wide range of directions. For example, while wolves preferentially follow the seismic lines cut into forested areas they also move off the lines and into surrounding forest. Similarly, butterflies do not take the steepest route during hilltopping, rather their flight pattern fluctuates [38]. Such behaviours can be accounted for by allowing q to take the form of a regular probability distribution over V.

In summary, we assume that q has the general form

$$q(x,.) \in L^2(V), \qquad q(x,v) \geq 0, \quad \int_V q(x,v)dv = 1\,. \tag{4}$$

With the above assumptions in place it is noteworthy to mention two statistical quantities later revealed to be of importance, the expectation and the variance-covariance matrix:

$$\mathbb{E}_q(x) = \int_V vq(x,v)dv, \qquad \mathbb{V}_q(x) = \int_V (v-\mathbb{E}_q(x))(v-\mathbb{E}_q(x))^T q(x,v)dv\,.$$

The product vv^T denotes the dyade product of two vectors and it defines a matrix. Other authors prefer to use tensorial notation such as $vv^T = v \otimes v$ [9, 10].

Furthermore, we consider potential restrictions on q that could result from distinct forms of environmental anisotropy. While information provided by magnetic cues, the sun and ocean currents could provide a unidirectional movement cue, topographical information in the form of roads, seismic lines and collagen fibres may only provide bidirectional anisotropy, i.e. animals or cells choose both directions with equal probability. In this latter case, we would assume symmetry of q,

$$q(x,-v) = q(x,v).$$

A direct consequence of this symmetry is

$$\mathbb{E}_q = 0 \quad \text{and} \quad \mathbb{V}_q(x) = \int_V vv^T q(x,v)dv.$$

3 The parabolic scaling

In this and the following two sections we discuss the three principal scalings: (i) parabolic scaling, (ii) hyperbolic scaling and (iii) moment closure. We will show that each of the methods have their own range of applicability, and that there are situations when one is favourable over the other. With the aim of making this methodology broadly accessible, we aim for transparent presentation by revealing all steps in the analysis, noting that such details are often omitted in the literature. To illustrate the structuring of what follows, the graphic (Figure 1) outlines the relationships between the scalings as they will be discussed in this manuscript. The parabolic limit (i) is found to play a pivotal role, as special cases of (ii) and of (iii) both lead back to (i). For readers less motivated by the technical aspects of what follows, we would like to note that each section is concluded with a summarising box and a comparison between the scalings is presented in Section 6.

3.1 Motivation of the parabolic limit

As illustrated in Figure 1, the parabolic limit marks a full-stop for scaling in our analyses, with all paths eventually leading to it. Given it's obvious and considerable importance to the modelling community, we therefore discuss this case first. Two ways to motivate the parabolic limit are (a) an appropriate scaling of space and time, and (b) large turning rates and large speeds of the particles. These two approaches are, in fact, equivalent, as we next illustrate.

E. coli bacteria on a petri-dish display an average turning rate of $\mu \approx 1/sec$ and an average speed of $s \approx 10^{-2} mm/sec$ (see [19]), whereas durations for experiments that investigate population level dynamics are typically of the order of hours or days. Taking a unit $U = 10000\,sec\,(\approx 3h)$, the turning rate and speed on this timescale become

$$\mu = 10^4 \frac{1}{U} \quad \text{and} \quad s = 10^2 \frac{mm}{U}.$$

Hence, introducing a small parameter

$$\varepsilon = 10^{-2},$$

we have

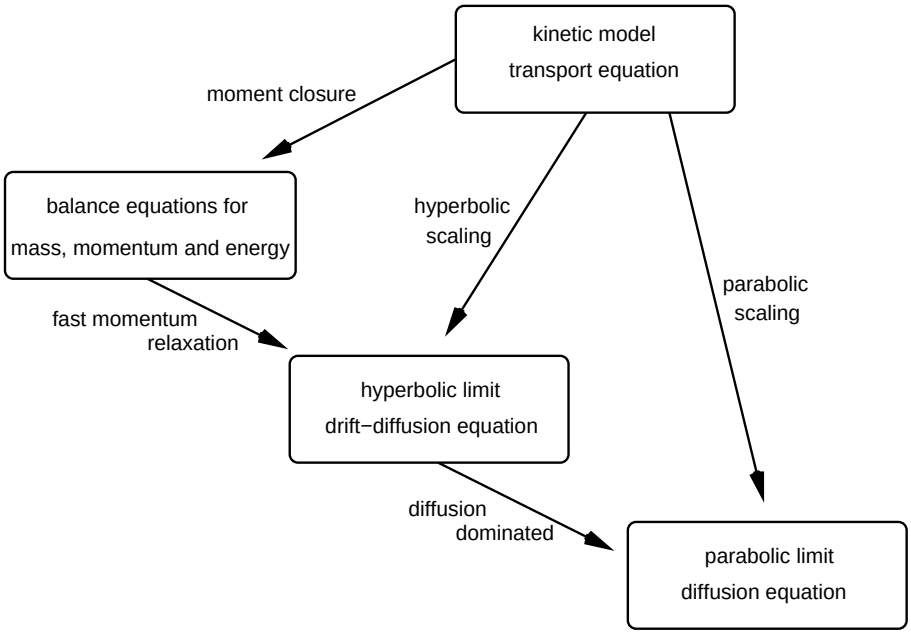

Fig. 1 Relations between the scalings and limit equations as discussed in the text.

$$\mu = O(\varepsilon^{-2}), \quad \text{and } s = O(\varepsilon^{-1}).$$

By writing $\mu = \varepsilon^{-2}\tilde{\mu}$ and $s = \varepsilon^{-1}\tilde{s}$ we obtain the equation

$$p_t + \varepsilon^{-1}\tilde{s}\theta \cdot \nabla p = \varepsilon^{-2}\tilde{\mu}(q\bar{p} - p),$$

where, for $v \in V$, we write $s\theta = v$ with $\theta \in \mathbb{S}^{n-1}$. Removing the ˜'s on the scaled parameters and rearranging we obtain

$$\varepsilon^2 p_t + \varepsilon v \cdot \nabla p = \mu(q\bar{p} - p). \tag{5}$$

Alternatively, we can simply introduce macroscopic time and space scales

$$\tau = \varepsilon^2 t, \qquad \xi = \varepsilon x$$

and rescale model (3) accordingly to obtain

$$\varepsilon^2 p_\tau + \varepsilon v \cdot \nabla_\xi p = \mu(q\bar{p} - p). \tag{6}$$

Formally, equations (5) and (6) are identical, though we note that we shall employ the second formulation with the new time and space coordinates (τ, ξ).

3.2 Parabolic limit in an oriented landscape

We first study the properties of the turning operator defined on $L^2(V)$:

$$\mathscr{L}\varphi(v) := \mu(q(x,v)\bar{\varphi} - \varphi).$$

The kernel of $\mathscr{L}$ is given by the linear space $\langle q(x,.)\rangle$. Hence we work in the weighted Lebesgue space $L^2_{q^{-1}}(V)$ where the inner product of a function f with q is given by

$$\int_V f(v)q(x,v)\frac{dv}{q(x,v)} = \int_V f(v)dv = \bar{f}.$$

On the complement set, $\langle q\rangle^\perp$, we can define a pseudo-inverse by solving the resolvent equation. Given a function $\psi \in \langle q\rangle^\perp$ we solve for $\phi \in \langle q\rangle^\perp$ such that

$$\mathscr{L}\phi = \psi. \tag{7}$$

Since $\phi, \psi \in \langle q\rangle^\perp$, we have $\bar{\phi} = \bar{\psi} = 0$ and the resolvent equation (7) reduces to

$$\phi = -\frac{1}{\mu}\psi. \tag{8}$$

where the pseudo-inverse appears as multiplication with $-\mu^{-1}$.

To analyse the scaled equation (6) we take the scaled coordinates (τ, ξ) and make a regular expansion in ε, called a *Hilbert expansion*:

$$p(\tau,\xi,v) = p_0(\tau,\xi,v) + \varepsilon p_1(\tau,\xi,v) + \varepsilon^2 p_2(\tau,\xi,v) + h.o.t.$$

Substituting into (6) and comparing orders of magnitude of ε:

- ε^0**:** The terms of leading order are $\mathscr{L}p_0(\tau,\xi,v) = 0$ which implies

$$p_0(\tau,\xi,v) = q(\xi,v)\bar{p_0}(\tau,\xi).$$

- ε^1**:** The terms of order one are

$$(\nabla\cdot v)p_0 = \mathscr{L}p_1\,.$$

This equation can be solved on $\langle q\rangle^\perp$, if the right hand side satisfies the solvability condition $(\nabla\cdot v)p_0 \in \langle q\rangle^\perp$. This condition reads

$$\int_V (\nabla\cdot v)q(\xi,v)p_0(\tau,\xi,v)\,\frac{dv}{q(\xi,v)} = \nabla\cdot\int_V vq(\xi,v)\,dv\,\bar{p_0}(\tau,\xi).$$

Crucially, this term is only equal to zero for arbitrary p_0 when we impose the following extra condition on q:

$$\mathbb{E}_q = \int_V vq(\xi,v)dv = 0. \tag{9}$$

We can then solve for the first order term and find

$$p_1(\tau,\xi,v) = -\frac{1}{\mu}\nabla\cdot v\, p_0(\tau,\xi,v).$$

- ε^2**:** The second order terms are

$$p_{0,\tau} + v\cdot\nabla p_1 = \mathscr{L} p_2.$$

From assumption (4) it follows that $\int_V \mathscr{L}\phi(v)dv = 0$ for all $\phi \in L^2_{q^{-1}}$. Hence we integrate the above equation and use index notation for summation over repeated indices:

$$\begin{aligned} 0 &= \int_V (p_{0,\tau} + v\cdot\nabla p_1)dv, \\ &= \bar{p}_{0,\tau} - \frac{1}{\mu}\int (v\cdot\nabla)(\nabla\cdot v)\,(\bar{p}_0(\tau,\xi)q(\xi,v))\; dv, \\ &= \bar{p}_{0,\tau} - \frac{1}{\mu}\partial_i\partial_j\left(\int_V v^i v^j q(\xi,v)\; dv\; \bar{p}_0(\tau,\xi)\right). \end{aligned}$$

This last equation can be written as a diffusion equation for the macroscopic density $\bar{p}_0(\tau,\xi)$:

$$\bar{p}_{0,\tau}(\tau,\xi) = \nabla\nabla(D(\xi)\bar{p}_0(\tau,\xi)). \tag{10}$$

with a macroscopic *diffusion tensor*

$$D(\xi) = \frac{1}{\mu}\int_V vv^T q(\xi,v)dv. \tag{11}$$

Since we assumed $\mathbb{E}_q = 0$ in (9), we find that the diffusion tensor for the particles is given by the variance-covariance matrix of the underlying fibre network:

$$D(\xi) = \frac{1}{\mu}\mathbb{V}_q(\xi).$$

With q assumed to be non-singular, the variance-covariance matrix $\mathbb{V}_q$ (and hence the diffusion tensor D) is positive definite and symmetric and equation (11) is uniformly parabolic.

We summarise this limit in the following result:

The Parabolic Scaling. In addition to (4) we make the following assumptions:

(A1)

$$\mathbb{E}_q = \int_V vq(x,v)dv = 0. \tag{12}$$

(A2) There exists a small parameter $\varepsilon > 0$ such that either

$$\mu = \varepsilon^{-2}\tilde{\mu}, \qquad s = \varepsilon^{-1}\tilde{s},$$

or

$$\tau = \varepsilon^2 t, \qquad \xi = \varepsilon x,$$

where $\tilde{\mu}, \tilde{s}, \tau, \xi$ are of order one.

Let $p(\tau,\xi,v)$ be a solution of the scaled kinetic equation

$$\varepsilon^2 p_\tau + \varepsilon v \cdot \nabla_\xi p = \mu(q\bar{p} - p). \tag{13}$$

Then the leading order term p_0 of a regular expansion $p = p_0 + \varepsilon p_1 + \varepsilon^2 p_2 + \ldots$ satisfies

$$p_0(\tau,\xi,v) = \bar{p}_0(\tau,\xi)q(\xi,v),$$

where $\bar{p}_0(\tau,\xi)$ is solution of the parabolic limit equation

$$\bar{p}_{0,\tau}(\tau,\xi) = \nabla\nabla(D(\xi)\bar{p}_0(\tau,\xi)) \qquad \left(= \partial_i\partial_j(D^{i,j}(\xi)p(\tau,\xi))\right) \tag{14}$$

with *diffusion tensor*

$$D(\xi) = \frac{1}{\mu}\int_V vv^T q(\xi,v)dv. \tag{15}$$

4 The hyperbolic scaling

The parabolic limit of the previous section considered macroscopic time and space scales, where time is scaled quadratically in ε and space linearly. For the parabolic limit to work it was necessary to specify $\mathbb{E}_q = 0$, with a diffusion equation arising. In the hyperbolic scaling we will observe that $\mathbb{E}_q$ corresponds to a drift term, which dominates when nonzero, and that in the hyperbolic limit we derive both a drift term and a diffusion correction[1] . For that, we assume that macroscopic time and space scales are both linear in ε, i.e.

$$\sigma = \varepsilon t, \quad \xi = \varepsilon x.$$

[1] This section is an adaptation of Section 4.1.3 from[17]. It was inspired by Dolak and Schmeiser [11] who apply this scaling to chemotactic movement and, while their results do not directly apply here, the methods are the same.

Under this rescaling, the transport equation (1) becomes

$$\varepsilon p_\sigma + \varepsilon(v\cdot\nabla)p = \mathscr{L}p. \tag{16}$$

Again, we use the operator properties of $\mathscr{L}$ on the space $L^2_{q^{-1}}(V)$ and split the solution into two parts (the *Chapman-Enskog expansion*):

$$p(\sigma,\xi,v) := \bar{p}(\sigma,\xi)q(\xi,v) + \varepsilon p^\perp(\sigma,\xi,v) \tag{17}$$

$$\text{with} \quad \int_V p^\perp(\sigma,\xi,v)q(\xi,v)\frac{dv}{q(\xi,v)} = \int_V p^\perp(\sigma,\xi,v)dv = 0.$$

Substituting the expansion (17) into (16) gives:

$$\begin{aligned}\varepsilon\bar{p}_\sigma q + \varepsilon^2 p^\perp_\sigma + \varepsilon(v\cdot\nabla)(\bar{p}q) + \varepsilon^2(v\cdot\nabla)p^\perp &= \mathscr{L}\left(\bar{p}q + \varepsilon p^\perp\right)\\ &= \varepsilon\mathscr{L}p^\perp.\end{aligned} \tag{18}$$

Integrating (18) over V and dividing by ε yields

$$\bar{p}_\sigma + \nabla\cdot\Big(\int_V vq\,dv\,\bar{p} + \varepsilon\int vp^\perp dv\Big) = 0, \tag{19}$$

where we used

$$\int_V p^\perp_\sigma dv = \frac{\partial}{\partial\sigma}\int_V p^\perp dv = 0.$$

Once again, the expectation of q appears

$$\bar{p}_\sigma + \nabla\cdot\Big(\mathbb{E}_q\bar{p} + \varepsilon\int_V vp^\perp dv\Big) = 0\,, \tag{20}$$

and to leading order this is the drift-dominated model

$$\bar{p}_\sigma + \nabla\cdot(\mathbb{E}_q\bar{p}) = 0, \tag{21}$$

where the drift velocity is given by the expectation of q.

We determine the next order correction term by constructing an approximation to $p^\perp$. From (20) we obtain $\bar{p}_\sigma$, substitute into (18) and divide by ε:

$$\begin{aligned}\mathscr{L}p^\perp &= -q\nabla\cdot\Big(\mathbb{E}_q\bar{p} + \varepsilon\int_V vp^\perp dv\Big) + \varepsilon p^\perp_\sigma + (v\cdot\nabla)(\bar{p}q) + \varepsilon(v\cdot\nabla)p^\perp\\ &= (v\cdot\nabla)(\bar{p}q) - q\nabla\cdot(\mathbb{E}_q\bar{p}) + O(\varepsilon).\end{aligned} \tag{22}$$

Hence to leading order we have:

$$\mathscr{L}p^\perp \approx q(v-\mathbb{E}_q)\cdot\nabla\bar{p} + (v\cdot\nabla q - q\nabla\cdot\mathbb{E}_q)\bar{p}. \tag{23}$$

To apply the pseudo-inverse of $\mathscr{L}$ on $\langle q\rangle^\perp$, we must check the solvability condition

$$\begin{aligned}\int_V \mathscr{L} p^\perp q \frac{dv}{q} &= \int_V \mathscr{L} p^\perp dv,\\ &\approx \nabla \bar{p} \cdot \int_V (q(v-\mathbb{E}_q)dv + \bar{p}\int_V (v\cdot\nabla q - q\nabla\cdot\mathbb{E}_q)dv,\\ &= \nabla\bar{p}\cdot(\mathbb{E}_q-\mathbb{E}_q) + \bar{p}\nabla\cdot(\mathbb{E}_q-\mathbb{E}_q),\\ &= 0.\end{aligned}$$

Hence we can apply the pseudo-inverse of $\mathscr{L}$ and find

$$p^\perp \approx -\frac{1}{\mu}\left(q(v-\mathbb{E}_q)\cdot\nabla\bar{p} + (v\cdot\nabla q - q\nabla\cdot\mathbb{E}_q)\bar{p}\right). \tag{24}$$

Substituting (24) into (20) we obtain

$$\begin{aligned}&\bar{p}_\sigma + \partial_j(\mathbb{E}_q^j\bar{p})\\ &= \frac{\varepsilon}{\mu}\partial_j\left(\int_V v^j\left[q(v^i-\mathbb{E}_q^i)\partial_i\bar{p} + (v^i\partial_i q - q\partial_i\mathbb{E}_q^i)\bar{p}\right]dv\right)\\ &= \frac{\varepsilon}{\mu}\partial_j\int_V v^j(v^i-\mathbb{E}_q^i)q\,dv\,\partial_i\bar{p}\\ &\quad + \frac{\varepsilon}{\mu}\partial_j\left(\left[\int_V v^j(v^i\partial_i q - q\int_V v'^i\partial_i q\,dv')dv\right]\bar{p}\right).\end{aligned}$$

The two integrals inside the square brackets can be written as

$$\begin{aligned}&\int_V v^j(v^i\partial_i q - q\int_V v'^i\partial_i q\,dv')dv\\ &= \int_V v^j v^i\partial_i q\,dv - \int_V v^j q\,dv\int_V v'^i\partial_i q\,dv'\\ &= \int_V (v^j-\mathbb{E}_q^j)v^i\partial_i q\,dv\\ &= \int_V (v-\mathbb{E}_q)\,v\cdot\nabla q\,dv,\end{aligned}$$

Hence we obtain

$$\begin{aligned}\bar{p}_\sigma + \nabla\cdot(\mathbb{E}_q\bar{p}) = \frac{\varepsilon}{\mu}\nabla\cdot\int_V v(v-\mathbb{E}_q)^T q\,dv\cdot\nabla\bar{p}\\ + \frac{\varepsilon}{\mu}\nabla\cdot\left(\left(\int_V (v-\mathbb{E}_q)(v\cdot\nabla q)dv\right)\bar{p}\right).\end{aligned} \tag{25}$$

We define the diffusion tensor D as before, i.e. as a multiple of the variance-covariance matrix of q:

$$D(x) := \frac{1}{\mu}\mathbb{V}_q = \frac{1}{\mu}\int_V (v-\mathbb{E}_q)(v-\mathbb{E}_q)^T q(x,v)dv. \tag{26}$$

We collect two properties of D:

$$\int_V v(v-\mathbb{E}_q)^T q(\xi,v)dv = \int_V (v-\mathbb{E}_q)(v-\mathbb{E}_q)^T q(\xi,v)dv = \mu D(\xi),$$

and

$$\begin{aligned}
\nabla\nabla(D\bar{p}) &= \partial_i\partial_j(D^{ij}\bar{p}) \\
&= \partial_i\partial_j\left(\frac{1}{\mu}\int_V v^i(v^j-\mathbb{E}_q^j)qdv\bar{p}\right) \\
&= \frac{1}{\mu}\partial_i\left(-\int v^i\partial_j\mathbb{E}_q^j\, qdv\bar{p}+\int v^i(v^j-\mathbb{E}_q^j)\partial_j q\, dv\bar{p}+\int v^i(v^j-\mathbb{E}_q^j)qdv\partial_j\bar{p}\right) \\
&= \frac{1}{\mu}\nabla\cdot\left(-\int v\,\mathrm{div}\mathbb{E}_q qdv\bar{p}+\int v(v-\mathbb{E}_q)\cdot\nabla qdv\bar{p}+\int v(v-\mathbb{E}_q)qdv\cdot\nabla p\right)
\end{aligned}$$

Then, with (25), we arrive at the limit equation with correction term

$$\bar{p}_\sigma+\nabla\cdot(\mathbb{E}_q\bar{p}) = \varepsilon\nabla\big(\nabla(D(\xi)\bar{p})+\frac{1}{\mu}\mathbb{E}_q(\nabla\cdot\mathbb{E}_q)\vec{p}\big). \tag{27}$$

Equivalently, we can use the moments of q to write the limit equation as

$$\bar{p}_\sigma+\nabla\cdot(\mathbb{E}_q\bar{p}) = \frac{\varepsilon}{\mu}\nabla\big(\nabla(\mathbb{V}_q(\xi)\bar{p})+\mathbb{E}_q(\nabla\cdot\mathbb{E}_q)\vec{p}\big). \tag{28}$$

Critically, if $\mathbb{E}_q\approx 0$ (as in the parabolic case) we obtain the same diffusion term as for the parabolic scaling in (14). In fact, for $\mathbb{E}_q=0$ we can simply rescale the hyperbolic limit equation (28) by $\tau=\varepsilon\sigma$ to obtain an identical limit to (14).

The Hyperbolic Scaling. Further to (4) we make the following assumptions:

(B1)
$$\sigma=\varepsilon t, \qquad \xi=\varepsilon x,$$
where σ,ξ are of order one.

Let $p(\sigma,\xi,v)$ be a solution of the scaled kinetic equation

$$\varepsilon p_\sigma+\varepsilon v\cdot\nabla_\xi p = \mu(q\bar{p}-p). \tag{29}$$

Then the solution p can be split into $p=\bar{p}q+\varepsilon p^\perp$, where the leading order term $\bar{p}(\sigma,\xi)$ is approximated by the solution of the drift-diffusion equation

$$\bar{p}_\sigma+\nabla\cdot(\mathbb{E}_q\bar{p}) = \frac{\varepsilon}{\mu}\nabla\big(\nabla(\mathbb{V}_q(\xi)\bar{p})+[\mathbb{E}_q(\nabla\cdot\mathbb{E}_q)]\bar{p}\big). \tag{30}$$

From the construction it is expected that the approximation should be second order in ε, although to our knowledge this has not yet been shown.

5 The moment approach

Moment closure provides a third way to derive macroscopic equations from the transport model (1). As in the previous cases, it was first developed in a physical context to describe the dynamics of fluids and gases and we will therefore adopt the physical definitions within the present biological context. The principle players are mass, momentum and energy, with the goal of defining model equations for these quantities [2].

Given a particle distribution $p(t,x,v)$, the mass is defined as

$$\bar{p}(t,x) = \int_V p(t,x,v)dv,$$

the momentum as

$$\bar{p}(t,x)U(t,x) := \int_V vp(t,x,v)dv,$$

and the internal energy by

$$E(t,x) = \int_V |v-U(t,x)|^2 p(t,x,v)dv.$$

The momentum implicitly defines the ensemble (or macroscopic) velocity

$$U(t,x) = \frac{1}{\bar{p}(t,x)} \int_V vp(t,x,v)dv.$$

The energy is the trace of the pressure tensor

$$\mathbb{P}(t,x) = \int_V (v-U(t,x))(v-U(t,x))^T p(t,x,v)dv,$$

in the sense that

$$E(t,x) = \text{tr}\, \mathbb{P}(t,x).$$

In a physical context mass, momentum and energy have very precise meanings yet applied to biology we must consider carefully their appropriate biological reinterpretation. The total mass, $\bar{p}$, and ensemble velocity, U, correspond directly to their physical quantities, describing respectively the total density of individuals and their average velocity. The momentum $\bar{p}U$ is somewhat different, since cells and animals generally cannot be regarded as hard spheres and hence $\bar{p}U$ is not the physical momentum an ensemble of cells would generate if it hits an object, for example. The biological momentum can simply be regarded as the average particle flux, i.e. the total density, $\bar{p}$, multiplied by the mean velocity, U. The energy is the trace of the full pressure tensor and direct interpretations of either pressure or energy are hard to find. We can, instead, consider these from a statistical perspective. The ratio $p/\bar{p}$

[2] This section is an adaptation from [10].

is a probability density with respect to the velocity, with $U/\bar{p}$ the expectation and $\mathbb{P}/\bar{p}$ the variance-covariance matrix. Consequently, $U/\bar{p}$ gives the mean velocity and $\mathbb{P}/\bar{p}$ gives information on the breadth of the distribution $p/\bar{p}$. The variance-covariance tensor $\mathbb{P}/\bar{p}$ is symmetric, but can be anisotropic and allowing greater spread in one direction than others. The energy $E/\bar{p}$ is the (magnitude of the) variance with $\sqrt{E/\bar{p}}$ the standard deviation.

We need one more variable which, in the physical context, corresponds to the energy flux:

$$Q(t,x) = \int_V |v-U(t,x)|^2 (v-U(t,x)) p(t,x,v) dv.$$

The vector Q is a trace of a full third order moment, with magnitude dominated by cells not moving with the mean velocity and direction given by the mean direction of the outliers, relative to the ensemble velocity U.

In a similar way, we can also define the ensemble pressure tensor of the system

$$\mathbb{P}_0(t,x) = \int_V U(t,x)U(t,x)^T p(t,x,v) dv = \bar{p}(t,x)U(t,x)U(t,x)^T$$

and the ensemble energy flux

$$Q_0(t,x) = \int_V U^2(t,x)U(t,x)p(t,x,v) dv = \bar{p}(t,x)U^2(t,x)U(t,x).$$

Next, we will derive differential equations for the macroscopic quantities mass, $\bar{p}$, momentum, $\bar{p}U$, and energy, E. To obtain the mass conservation equation, we simply integrate (3) over V to obtain

$$\bar{p}_t(x,t) + \nabla \cdot (\bar{p}(t,x)U(t,x)) = 0\,. \tag{31}$$

The momentum equation is derived through multiplication of (3) by v and integrating (omitting space, time and v dependencies for clarity):

$$\begin{aligned} \int_V v p_t \, dv + \int_V v(v\cdot\nabla)p \, dv &= \mu \int_V vq \, dv \, \bar{p} - \mu \int_V vp \, dv, \\ (\bar{p}U)_t + \nabla \cdot \int_V vv^T p dv &= \mu \bar{p}\mathbb{E}_q - \mu \bar{p}U\,. \end{aligned} \tag{32}$$

The pressure tensor can be written as

$$\begin{aligned} \mathbb{P} &= \int_V (v-U)(v-U)^T p \, dv, \\ &= \int vv^T p \, dv - \int Uv^T p \, dv - \int vU^T p \, dv + \int UU^T p \, dv, \\ &= \int vv^T p \, dv - \bar{p}UU^T. \end{aligned} \tag{33}$$

We use this expression in (32) and obtain the momentum equation

$$(\bar{p}U)_t + \nabla\cdot(\bar{p}UU^T) = -\nabla\mathbb{P} + \mu(\bar{p}\mathbb{E}_q - \bar{p}U). \tag{34}$$

For the energy equation, we multiply (3) by v^2 and integrate:

$$\begin{aligned}\int v^2 p_t dv + \int v^2 (v\cdot\nabla) p\, dv &= \mu \int v^2 q\, dv\, \bar{p} - \mu \int v^2 p\, dv,\\ E_t + \nabla\cdot\int v v^2 p\, dv &= \mu\int v^2 q\, dv\, \bar{p} - \mu E\,.\end{aligned} \tag{35}$$

We study the two integral terms in (35) separately. To obtain an expression for $\int vv^2 p$, we study the heat flux Q:

$$\begin{aligned}Q &= \int |v-U|^2 (v-U) p\, dv,\\ &= \int vv^2 p dv - \int v^2 U p dv - \int 2(vU) v p dv\\ &\quad + \int 2(vU) U p dv + \int U^2 v p dv - \int U^2 U p dv,\\ &= \int vv^2 p dv - UE - 2U\cdot\int vv^T p dv + 2U\cdot(\bar{p}UU^T),\\ &= \int vv^2 p dv - UE - 2U\cdot\mathbb{P},\end{aligned} \tag{36}$$

where we used (33) in the last equality.

To obtain the second order q term, we compute

$$\begin{aligned}\text{tr}\,\mathbb{V}_q &= \int_V (v^i - \mathbb{E}_q^i)(v_i - \mathbb{E}_{qi}) q\, dv,\\ &= \int v^i v_i q dv - \int v^i \mathbb{E}_{qi} q dv - \int \mathbb{E}_q^i v_i q dv + \int \mathbb{E}_q^i \mathbb{E}_{qi} q dv,\\ &= \int v^2 q dv - \mathbb{E}_q^2.\end{aligned} \tag{37}$$

Hence the energy equation (35) becomes

$$E_t + \nabla\cdot(EU) = -\nabla Q - 2\nabla\cdot(U\cdot\mathbb{P}) + \mu(\text{tr}\,\mathbb{V}_q + \mathbb{E}_q^2 - E). \tag{38}$$

The equations for mass, $\bar{p}$, momentum, $\bar{p}U$, and energy, E, are given by (31, 34, 38) respectively. However, this system is not closed, due to the inclusion of the higher order moments $\mathbb{P}$ and Q. To resolve this, we can attempt a derivation of differential equations for these higher moments, although in doing so even higher order moments will appear: if fact, the sequence of moment equations is unending and we face a *moment closure problem*. Thus, we must find a mechanism for estimating the higher order moments in order to close the system of equations (31, 34, 38). Two standard ways of finding a moment closure are through (1) the equilibrium distribution and (2) entropy maximisation. Here we focus on the first method, noting that details of the entropy method can be found elsewhere (e.g. [16]).

5.1 Moment closure

The principal assumption here is that the system is close to equilibrium and that the higher order moments are dominated by this equilibrium. Earlier, we computed $\ker \mathscr{L} = \langle q \rangle$. Hence the equilibrium distribution has the form

$$p_e(t,x,v) = \bar{p}(t,x)q(x,v).$$

For this distribution, we can explicitly compute the moments:

- mass,
$$\bar{p_e}(t,x) = \int \bar{p}(t,x)q(x,v) = \bar{p}(t,x);$$
- momentum,
$$\bar{p_e}(t,x)U_e(t,x) = \int v\bar{p}(t,x)q(x,v)dv = \bar{p}(t,x)\mathbb{E}_q(x);$$
- pressure tensor,
$$\mathbb{P}_e(t,x) = \int (v-\mathbb{E}_q)(v-\mathbb{E}_q)^T \bar{p}(t,x)q(x,v)dv = \bar{p}(t,x)\mathbb{V}_q(x); \tag{39}$$
- energy flow,
$$Q_e(t,x) = \int |v|^2 v\bar{p}(t,x)q(x,v)dv = \bar{p}(t,x)\mathbb{T}_q(x), \tag{40}$$
where we introduce the third order moment of q
$$\mathbb{T}_q(x) = \int v^2 vq(x,v)dv.$$

These formulae reveal that at equilibrium all momentum is carried by the ensemble, which is moving in the mean network direction $\mathbb{E}_q$, and that all energy and pressure is produced by the variance-covariance matrix of the underlying distribution. The above expressions for the pressure tensor and energy flux are employed to close system (31, 34, 38) for mass, momentum, and energy. We should stress that here *we are making an approximation* and that even though we retain the equality sign $\bar{p}, U, E$ are *approximations* to the exact $\bar{p}, U, E$ values.

Moment Closure. In addition to (4) we assume that

(C1) the macroscopic quantities $\mathbb{P}$ and Q are given by their equilibrium distributions (39, 40).

Then the mass $\bar{p}$, the momentum $\bar{p}U$ and the energy E are approximated by the solution of the closed system:

$$\bar{p}_t + \nabla(\bar{p}U) = 0 \tag{41}$$

$$(\bar{p}U)_t + \nabla\cdot(\bar{p}UU^T) = -\nabla(\bar{p}\mathbb{V}_q) + \mu(\bar{p}\mathbb{E}_q - \bar{p}U) \tag{42}$$

$$E_t + \nabla\cdot(EU) = -\nabla(\bar{p}\mathbb{T}_q) - 2\nabla\cdot(U\cdot(\bar{p}\mathbb{V}_q)) + \mu(\operatorname{tr}\mathbb{V}_q + \mathbb{E}_q^2 - E) \tag{43}$$

We note that for the closed system (41, 42, 43), the first two equations are independent of the energy E. Hence, equation (43) decouples and we can study the first two equations (41) and (42) independently.

5.2 Fast flux relaxation

The derivatives on the left hand side of equations (41, 42, 43) all have characteristic form $\partial_t\phi + \nabla\cdot(U\phi)$, termed the directional derivative of ϕ in the direction of the flow U (also known as the material derivative or characteristic derivative). As a special case we assume that the flux relaxes quickly to its equilibrium, i.e. we set

$$0 = -\nabla(\bar{p}\mathbb{V}_q) + \mu(\bar{p}\mathbb{E}_q - \bar{p}U),$$

which we can solve for $\bar{p}U$ to give

$$\bar{p}U = -\frac{1}{\mu}\nabla(\bar{p}\mathbb{V}_q) + \bar{p}\mathbb{E}_q.$$

Using this expression in (41) yields the drift-diffusion equation

$$\bar{p}_t + \nabla(\bar{p}\mathbb{E}_q) = \frac{1}{\mu}\nabla\nabla(\bar{p}\mathbb{V}_q). \tag{44}$$

Fast Flux Relaxation. In addition to (4) we assume that:

(C1) the macroscopic quantities $\mathbb{P}$ and Q are given by the equilibrium distributions as in (39, 40);
(C2) the momentum $\bar{p}U$ relaxes fast to its equilibrium.

Then the total mass $\bar{p}(t,x)$ is approximated by the solution of the drift-diffusion limit equation

$$\bar{p}_t + \nabla(\bar{p}\mathbb{E}_q) = \frac{1}{\mu}\nabla\nabla(\bar{p}\mathbb{V}_q). \tag{45}$$

6 Comparison between scalings

In this section we will summarise the various scaling methods and compare and contrast our findings. First we will focus on the forms of the limit equations themselves, with an explanation of the relationships between them, before proceeding to examine their underlying assumptions. For convenience of comparison, we unify the notation by setting $u = \bar{p} = \bar{p}_0$ and specifying a generic time coordinate t (noting that t had been rescaled to τ for the derivation of the parabolic and hyperbolic limits).

6.1 Relationships between limit equations

The three scaling approaches resulted in the following four limit equations:

- Parabolic scaling (PS),
$$u_t = \frac{1}{\mu}\nabla\nabla(\mathbb{V}_q u); \tag{PS}$$
- Hyperbolic scaling (HS),
$$u_t + \nabla\cdot(\mathbb{E}_q u) = 0; \tag{HS}$$
- Hyperbolic scaling with correction terms (HC),
$$u_t + \nabla\cdot(\mathbb{E}_q u) = \frac{\varepsilon}{\mu}\nabla\nabla(\mathbb{V}_q u) + \frac{\varepsilon}{\mu}\nabla\cdot(\mathbb{E}_q(\nabla\cdot\mathbb{E}_q)u); \tag{HC}$$
- Moment closure (MC),
$$u_t + \nabla(\mathbb{E}_q u) = \frac{1}{\mu}\nabla\nabla(\mathbb{V}_q u). \tag{MC}$$

Clearly the above equations reveal significant overlap. For example, moment closure (*MC*) is a combination of the parabolic (*PS*) and hyperbolic scaling (*HS*), containing

both diffusion and drift terms. Consequently, we refer to the parabolic scaling as the *diffusion-dominated* case, with the hyperbolic scaling the *drift-dominated* case. More formally, the relationships between the limiting equations can be grouped into the following lemma.

Lemma 1. *We summarise the relationships into five scenarios.*

1. **(Diffusion-dominated)** *In the case $\mathbb{E}_q = 0$ all three approaches (PS,HC,MC) lead to the parabolic limit (PS), while (HS) is trivial.*
2. **(Diffusion-dominated)** *If $\mathbb{E}_q \approx O(\varepsilon^2)$, then equations (HC) and (MC) coincide with the parabolic limit (PS) to order ε.*
3. **(Drift-diffusion limit)** *If $\mathbb{E}_q \approx O(\varepsilon)$ equation (HC) is identical to (MC) to leading order (assuming a suitable scaling of time in (HC)).*
4. **(Drift-dominated)** *If $\mathbb{V}_q \approx O(\varepsilon)$, then (MC) coincides with the hyperbolic scaling (HS) to leading order.*
5. **(Drift-dominated)** *If $\mu \approx O(\varepsilon^{-1})$, then (MC) once again coincides with (HS) to leading order.*

6.2 Assumptions behind limit equations

Having explored the relationships behind the limit equations, we next consider their underlying assumptions.

(Parabolic) Here the expectation $\mathbb{E}_q = 0$ and there exists a small parameter $\varepsilon > 0$ such that either $\tau = \varepsilon^2 t, \xi = \varepsilon x$, where τ and ξ are both of order one, or $\mu = \varepsilon^{-2}\tilde{\mu}, s = \varepsilon^{-1}\tilde{s}$, where $\tilde{\mu}$ and $\tilde{s}$ are both of order one.
(Hyperbolic) There exists a small parameter $\varepsilon > 0$ such that $\sigma = \varepsilon t, \xi = \varepsilon x$, where σ and ξ are both of order one.
(Moments) The higher moments $\mathbb{P}$ and Q are given by the equilibrium distribution and the momentum ρU relaxes quickly.

While an all-encompassing interpretation of these assumptions is somewhat difficult, we provide the following intuitive scenarios. In the following section, these distinctions will be illuminated further through specific applications.

(Parabolic) The time scale is one in which particles are fast and turn frequently, with movement close to a Brownian random movement. The environment provides no specific directional cue (or, at least, a relatively weak directional cue) and hence $\mathbb{E}_q \simeq 0$ (i.e. movement up or down a given direction is effectively equal). Directional bias is included through possible anisotropy of the variance-covariance tensor $\mathbb{V}_q$ of the underlying medium.
(Hyperbolic) Once again, time and space scales are chosen such that particles are fast and turn often. But now the movement has a very clear directional component, $\mathbb{E}_q \neq 0$ and the drift component dominates.

(Moments) Here it is assumed that the pressure tensor is close to the pressure tensor of the equilibrium. Effectively, the system as a whole is near to equilibrium with subsequently small differential pressure terms. This implies that the population density p is "somewhat" closely aligned with the underlying tissue.

We note that all three methods lead to an anisotropic diffusion equation of the form

$$U_t = \nabla\nabla(DU) \tag{46}$$

i.e. the diffusion tensor lies inside the two derivatives. In the literature, anisotropic diffusion is usually associated with an equation in divergence form,

$$V_t = \nabla(D\nabla V). \tag{47}$$

This second form is derived from material physics, where the material flux is taken to be proportional to the gradient ∇V with proportionality factor D. As we also discuss in section 7.1.3 below, the above two models are quite different. If D is positive definite, equation (47) obeys the maximum principle and solutions converge to homogeneous steady states (on bounded domains with zero-flux boundary conditions, for example). In contrast, equation (46) does not have a maximum principle and, as we see later, spatial patterns can evolve.

When deriving diffusion equations from stochastic processes, both of the above versions (46) and (47) can be generated. For example, Othmer and Stevens [35] present a careful analysis that reveals how different assumptions for an individual's local response to the environment results in distinct macroscopic models, including the above two forms. Here we have shown how a model of type (46) arises very naturally. It is certainly possible that a distinct set of assumptions to those used in this paper could also give rise to a model of type (47), however we do not take this further at present.

7 Examples and applications

During the last few sections we have established a toolkit for generating distinct macroscopic equations, originating from the same transport model for movement of an individual (whether cell or organism) in an oriented environment. In this section we demonstrate these findings through a combination of examples and some specific applications.

7.1 Bidirectional and nondirectional environments

Here we consider environments in which the orientational cues do not provide a single direction to the biased movement. Examples range from the movement of

wolves along seismic lines, hikers along footpaths, animals along roads or cells along collagen fibres: i.e., while there is a tendency to move with the alignment of the environment, there is no specific "up" or "down". As previously specified, we model this by assuming symmetry in q:

$$q(x,-v) = q(x,v)\,,$$

with the direct consequence

$$\mathbb{E}_q = 0 \quad \text{and} \quad \mathbb{V}_q(x) = \int_V vv^T q(x,v)dv\,.$$

In relation to the above scaling methods, Item 1. of Lemma 1 applies: we have no drift term and all methods lead (eventually) to the diffusion limit

$$\bar{p_t} = \nabla(\nabla D(x)\bar{p})\,, \tag{48}$$

where $D(x) = \frac{1}{\mu}\mathbb{V}_q(x)$ is an anisotropic diffusion tensor.

7.1.1 Isotropic diffusion: the Pearson walk

We illustrate the above with the simplest version of a transport process as expressed by (3) in a completely uniform directional field (i.e. we have a nondirectional environment): the Pearson walk. Individuals are assumed to move with a constant speed s ($V = s\mathbb{S}^{n-1}$) and the underlying directional field is uniform:

$$q(x,v) = \frac{1}{|V|} = \frac{s^{1-n}}{|\mathbb{S}^{n-1}|}.$$

Again, q is symmetric and hence $\mathbb{E}_q = 0$. The variance is computed as

$$\mathbb{V}_q = \int vv^T q(v)dv = \frac{s^{1-n}}{|\mathbb{S}^{n-1}|}s^2 s^{n-1}\int_{\mathbb{S}^{n-1}} \gamma\gamma^T d\sigma = \frac{s^2}{|\mathbb{S}^{n-1}|}\frac{|\mathbb{S}^{n-1}|}{n}\mathbb{I}_n = \frac{s^2}{n}\mathbb{I}_n,$$

where $\mathbb{I}_n$ denotes the identity matrix.

Hence, the drift component will be zero and the diffusion is isotropic with diffusion constant[3]

$$d = \frac{s^2}{\mu n}.$$

[3] A general formula for directional moments, such as $\int \gamma\gamma^T d\gamma = |\mathbb{S}^{n-1}|/n\,\mathbb{I}_n$ can be found in Hillen [16].

7.1.2 Anisotropic diffusion example

We present a specific example together with some simulations of the transport model and its diffusive limit. Specifically, we consider a migrating population within a simple rectangular landscape (set to be of dimensions $[-10,10]\times[-10,10]$) with an oriented section centring on the origin. The orientational field strength is assumed to reduce with distance, effectively becoming isotropic in the periphery. See Figure 2A-D for a representation of this environment.

For the directional distribution q we consider the bimodal von Mises distribution:

$$q(x,\theta) = \frac{1}{4\pi I_0(k)}\left(e^{k\theta\cdot\gamma} + e^{-k\theta\cdot\gamma}\right), \tag{49}$$

where $\theta \in \mathbb{S}^1$ defines the movement direction of the population and $\gamma \in \mathbb{S}^1$ defines the dominating alignment of the local environment. I_n denotes the modified Bessel function of first kind of order n. Note that the von Mises distribution is the analogue of a normal distribution on a circle. The parameter k defines the strength of anisotropy and is termed the *parameter of concentration*. The above bimodal von Mises distribution clearly has two local maxima, one for $\theta = \gamma$ and one for $\theta = -\gamma$ [3]. For $k \to 0$ it converges to a uniform distribution (i.e. isotropic), while for $k \to \infty$ it converges to a sum of two point measures in directions γ and $-\gamma$.

To represent an environment in which anisotropy varies in the manner described, we assume $k(x)$ decays exponentially with distance from the origin

$$k(x) = k_0 e^{-r|x|^2},$$

where, in this example, we set $k_0 = 10$ and $r = 0.25$. This leads to high anisotropy in the centre of the domain and almost no directional bias in the periphery. Generally, γ could vary in space (for example, as in a curving road) however here we set it constant and in the direction of the diagonal, $\gamma(x) = (1/\sqrt{2}, 1/\sqrt{2})^T$. Figure 2A represents the environmental anisotropy for the central portion of the field, with the orientation and size of k represented by the direction and length of the individual line segments. For the three field positions indicated we plot the corresponding bimodal von Mises distributions in 2B-2D.

We first simulate the original transport model by substituting the above k and γ into (49) and solving equation (3). For details of the numerical methods used throughout this section, we refer to the Appendix. We assume the population is initially homogeneous and unaligned, with $p(x,v,0) = \text{constant}$ and $\bar{p}(x,0) = 1$. To limit the impact from boundaries we impose periodic boundary conditions along edges. In Figure 2E-G we plot the macroscopic cell density $\bar{p}(x,t)$ at $t = 50$ for three distinct speeds, s, and turning rate, μ: (E) $s = 0.1, \mu = 0.01$; (F) $s = 1, \mu = 1$; (G) $s = 10, \mu = 100$. Note that the parabolic limit corresponds to the limiting scenario in which $s \to \infty$, $\mu \to \infty$ with s^2/μ constant and we can therefore expect (G) to most accurately reflect the solution to the parabolic model. The simulations reveal the impact of the environmental anisotropy on the population. Far from the origin

the population is almost uniformly distributed. Nearer the centre a heterogeneous population distribution arises due to movement into the aligned region with subsequent transport in the direction of alignment. The bidirectional movement in this region results in symmetry in the population distribution, with a "dumbbell-like" pattern arising composed from regions of higher and lower density. The aggregations develop due to transport along the aligned region where they accumulate in the peripheral, isotropic regions. Notice that there is no taxis or adhesion involved in these aggregations; the patterns result solely from the geometry of the underlying network.

We next determine the corresponding drift ($\mathbb{E}_q$) and diffusion ($\mathbb{V}_q$) for the macroscopic equations by finding the moments of the bimodal von Mises distribution. Such computations are usually quite involved and require multiple trigonometric integrals (see [30]), however in the Appendix we present an alternative method based on the divergence theorem. Specifically, we find

$$\begin{aligned}\mathbb{E}_q(x) &= 0\,,\\ \mathbb{V}_q(x) &= \frac{1}{2}\left(1-\frac{I_2(k(x))}{I_0(k(x))}\right)\mathbb{I}_2+\frac{I_2(k(x))}{I_0(k(x))}\gamma\gamma^T\,.\end{aligned} \tag{50}$$

Thus, as expected for the bidirectional case, the drift term disappears while diffusion generates a tensor composed from an isotropic ($\mathbb{I}_2$-term) and non-isotropic component ($\gamma\gamma^T$-term). Consequently, the macroscopic version of the transport equation simulated above is the anisotropic diffusion equation

$$\bar{p_t} = \frac{s^2}{\mu}\nabla(\nabla\mathbb{V}_q(x)\bar{p})\,, \tag{51}$$

where the heterogeneous and anisotropic diffusion tensor is given by (50) using the choices for γ and $k(x)$ above that define our direction distribution. Simulations are shown in Figure 2H for a simulation of (51) with $s^2/\mu = 1$, with $\bar{p}(x,t)$ plotted at $t = 50$. Notably, the population distribution quantitatively matches the output from the transport model under the simulated parabolic limit scaling of s and μ.

7.1.3 Steady states

The above simulations suggest a capacity of the model to generate inhomogeneous steady states, at first a little surprising for a pure diffusion model. Closer scrutiny of (51) reveals how these patterns could arise as we demonstrate through the one-dimensional example. Consider the following distinct models for movement of a population within an interval:

$$u_t = (d(x)u_x)_x \tag{52}$$

and

$$u_t = (d(x)u)_{xx} \tag{53}$$

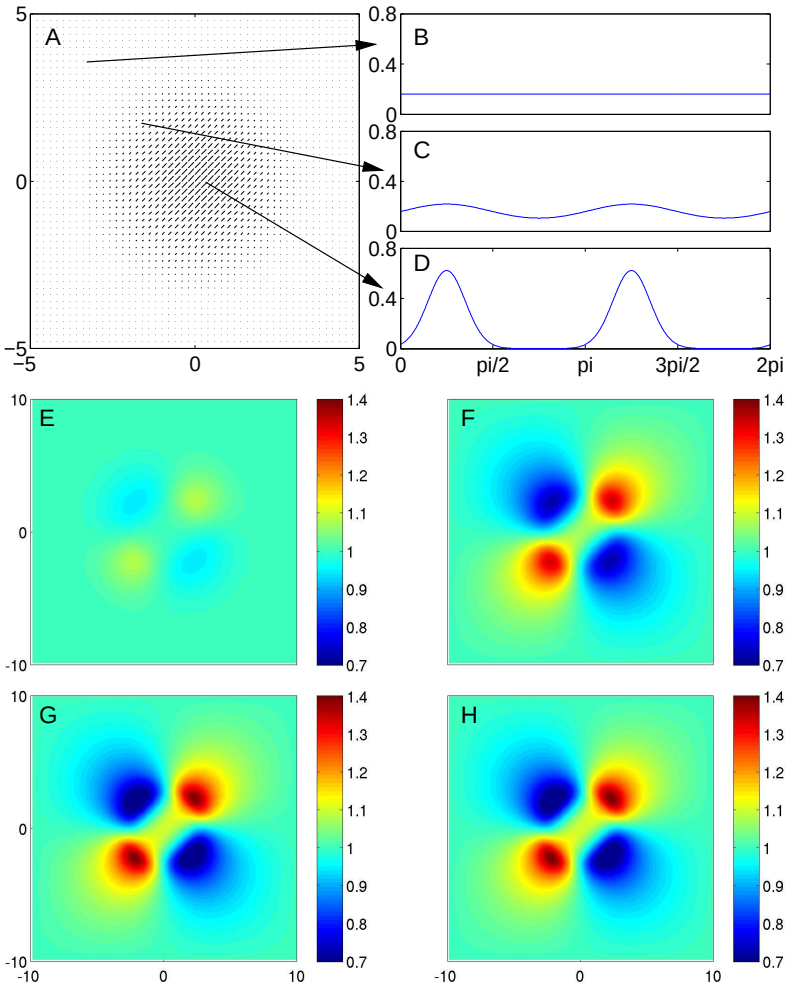

Fig. 2 Population heterogeneity arising due to bidirectional orientation of the environment. (A)-(D) representation of the imposed anisotropy, with (A) representing strength of anisotropy k (length of line segments) and alignment in the field (figure truncated at ± 5 to aid clarity of presentation) and (B)-(D) plotting the corresponding distribution (49) at each point indicated, as a function of $\theta = (\cos\phi, \sin\phi)$ for $\phi \in [0, 2\pi)$. Note that two dominating and equal orientations arise corresponding to $\gamma = \pm(\sqrt{2}/2, \sqrt{2}/2)$. (E)-(G) Simulation of the transport model (3) under the imposed q, showing the predicted macroscopic cell density $\bar{p}$ at time $t = 50$ for (E) $s = 0.1, \mu = 0.01$; (F) $s = 1, \mu = 1$; (G) $s = 10, \mu = 100$. (H) Simulation of the parabolic limit (51) at the same time $t = 50$ with $s^2/\mu = 1$ and the diffusion tensor as computed from (50). For details of the numerical implementations we refer to the Appendix.

with homogeneous Neumann conditions assumed at the boundaries. Equation (53) can be expanded into $u_t = (d'(x)u + d(x)u_x)_x$, revealing an additional advective term with advective velocity d' in comparison to (52). To determine the impact of this extra term we examine steady states for (52) and (53).

At steady state, Equation (52) leads to $(d(x)u_x)_x = 0$ which, after integrating and applying the boundary conditions, yields $d(x)u_x = 0$. This implies $u_x = 0$ and $u(x)$ is constant at steady state. This is what we expect for a pure diffusion process. Steady states for (53), on the other hand, satisfy $(d(x)u)_{xx} = 0$ and hence we find $(d(x)u)_x = 0$. Thus, $d(x)u = c$ (constant) and

$$u(x) = \frac{c}{d(x)}.$$

For spatially varying $d(x)$, equation (53) clearly allows nonuniform steady states, with the corresponding $u(x)$ being high or low in small or large diffusion regions, respectively. The additional advective term lies at the heart of this nontrivial steady state.

7.1.4 Application to seismic line following

Having confirmed that the diffusion model (51) can accurately capture predicted behaviour of the original transport model, at least under relevant scalings, we now apply the method to tackle a specific ecological problem: wolf movement in certain habitats. The model as discussed is particularly useful for describing the movements of populations in environments containing linear features such as roads, rivers, valleys, or seismic lines. Work by McKenzie and others [30, 31] determined the movement patterns of wolves in a typical Western Canadian habitat, consisting of boreal forest cut by seismic lines. Seismic lines are clear-cut straight lines (with a width of about 5m) used by oil exploration companies for testing of oil reservoirs. Typical densities are approximately $3.8\,km$ of lines on $1\,km^2$ and both wolves and ungulates (such as caribou) use these lines to move and forage, leading to significant impact on predator prey-interactions.

To describe the movement of wolves in such a habitat, McKenzie used GPS data generated from 4 individual wolves and estimated parameters for a diffusion-advection model, dividing the habitat into three areas: (i) seismic lines, (ii) near seismic lines (less or equal 50 m), and (iii) far from seismic lines (larger than 50m). Wolves demonstrated preferred movement along lines, while occasionally leaving lines to reenter forest. In particular, wolf movement data on seismic lines supported a fit to the directional distribution given by the bimodal von Mises distribution (49), where $\gamma(x) \in \mathbb{S}^1$ now describes the direction of the seismic line and $\theta \in \mathbb{S}^1$ the movement direction of the wolves.

To model this scenario we consider the parabolic limit of an underlying transport model in which wolf direction varies according to being on or off a seismic line. With no up or down information provided by the seismic line, we therefore have a bidirectional local environment and can expect the density of wolves, $w(x,t)$, to

follow the anisotropic diffusion equation

$$w_t = \frac{s^2}{\mu}\nabla(\nabla\mathbb{V}_q w)\,, \tag{54}$$

where the anisotropic diffusion tensor $\mathbb{V}_q$ is given by equation (50), $\gamma(x)$ will correspond to the direction of a seismic line while $k(x)$ varies according to a position on or off a seismic line.

To illustrate the applicability, consider for the moment a coordinate system aligned with a seismic line, i.e. $\gamma = e_1$. Here we can directly compute the diffusion tensor:

$$\mathbb{V}_{\tilde{q}} = \begin{pmatrix} \frac{1}{2}\left(1+\frac{I_2(k)}{I_0(k)}\right) & 0 \\ 0 & \frac{1}{2}\left(1-\frac{I_2(k)}{I_0(k)}\right) \end{pmatrix}.$$

The term $I_2(k)/I_0(k)$ enhances the mobility along a seismic line and reduces mobility in perpendicular direction. Moreover, for $k \to \infty$ (corresponding to an increasing strength of anisotropy), $I_2(k)/I_0(k) \to 1$ and the above diffusion tensor collapses to one-dimensional diffusion along the seismic line.

Away from the seismic lines wolves show no clear tendency to migrate towards or away from seismic lines [30]. Effectively, away from the lines we set $k(x) = 0$ in the bimodal von Mises distribution (49) and we obtain the isotropic diffusion tensor:

$$\mathbb{V}_{\tilde{q}} = \frac{1}{2}\mathbb{I}_2. \tag{55}$$

Using these ideas, we next simulate the expected population distribution for wolves in a typical habitat containing seismic lines. The aerial photograph in Figure 3A is of a Northern Alberta landscape in winter, demonstrating a woodland habitat criss-crossed with a combination of roads (thicker lines) and seismic lines (thinner lines). This image was digitised into a binary map, Figure 3B, showing areas of seismic lines (or roads) (white) and away from seismic lines (black). An automated processing of this image was applied to calculate the orientation at a point specified as seismic line, with this orientation determining the vector field $\gamma(x)$ used to compute the anisotropic diffusion tensor (50). In Figure 3C this anisotropy is represented for a small square section indicated by the boxed area in 3B, with the long axes at each point representing the direction (and strength) of the alignment. We set $k = 2.5$ for points marked as on a seismic line and $k = 0$ for points marked as off a seismic line. To limit the impact from boundary conditions we remark that the digitised region in B was buffered with a perimeter of isotropic diffusion.

Preliminary simulations for the distribution of wolves, w, are shown for two initial conditions: a uniform distribution $w(x,0) = 1$ in Figure 3D-F and a 2D Gaussian-type distribution centered in the field for 3G-I, $w(x,0) = 100e^{-|x-x_c|^2}$. In the former we observe the emergence of a spatially variable wolf population from homogeneity, with a clear tendency of the population to accumulate and move preferentially along the lines, shown at times (D) $t = 0$, (E) $t = 1$ and (F) $t = 10$. The diffusion from the concentrated initial distribution further reveals this preferential spread, with wolves

clearly dispersing more rapidly along the lines than through the surrounding lines; here, wolf distribution is shown at (G) $t = 0$, (H) $t = 1$ and (I) $t = 5$.

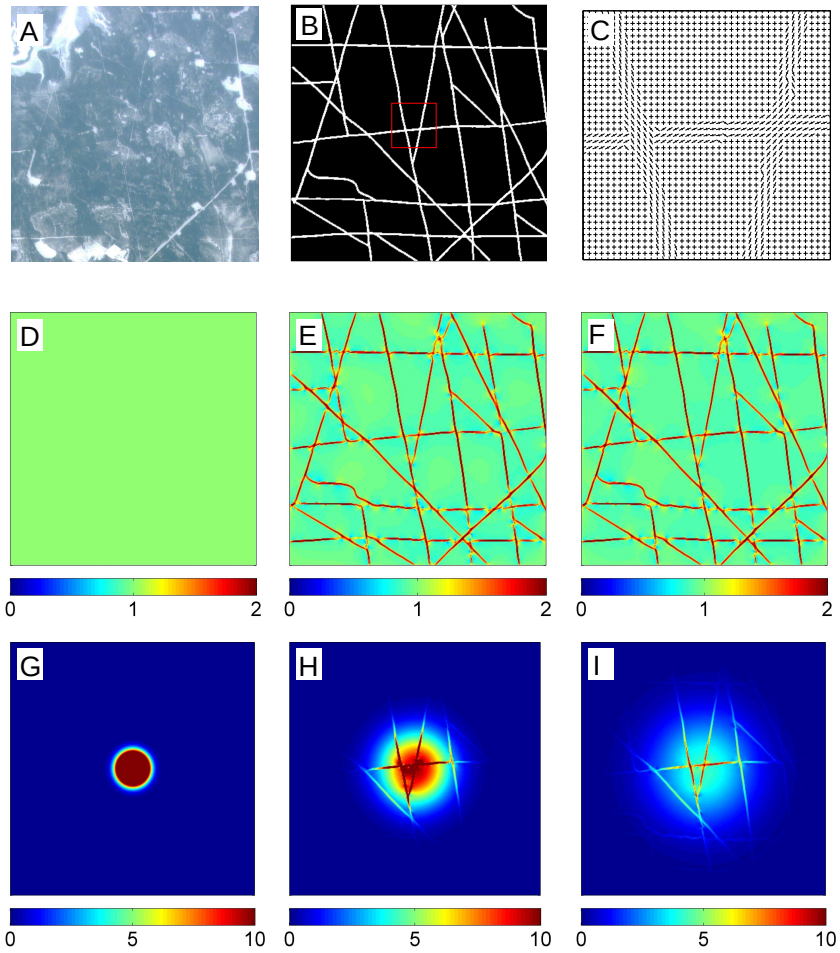

Fig. 3 Wolf distribution in anisotropic environments. (A) Aerial photograph of a Northern Alberta (Canada) landscape, showing criss-crossing seismic lines and roads. (B) Binary map created from (A) with lines marked as white. (C) Blow-up of boxed region in (B), showing detail of the anisotropic diffusion tensor automatically generated from the image in (B). (D-F) Numerical simulation of equation (54) for a uniform distribution $w(x,0) = 1$, using the computed diffusion tensor generated from (B) and setting $s^2/\mu = 1$. Wolf density $w(x,t)$ is plotted at times (D) $t = 0$, (E) $t = 1$ and (F) $t = 10$. (G-I). Numerical simulation for $w(x,0) = 100e^{-|x-x_c|^2}$ (where x_c marks the domain centre), showing $w(x,t)$ at times (G) $t = 0$, (H) $t = 1$ and (I) $t = 5$. Note that the simulated domain is a little larger than that plotted, with the surrounding zone assumed isotropic and implemented to reduce the impact of boundary conditions (note that this has negligible impact on the qualitative results presented). For details of the numerical implementation we refer to the Appendix.

7.2 Unidirectional environments

In many cases an environmental cue can provide a specific direction, as in the magnetic fields used by migrating turtles and whales, the slope of the ground for hilltopping butterflies, the movement of organisms towards food sources or the current of a river. To include such cues we can remove the symmetry assumption for q imposed in the bidirectional case.

To examine how this impacts on the scaling limit we consider the specific example of attraction to a food supply. We let $F(x)$ denote a given food distribution, with $x \in \mathbb{R}^2$, and assume that individuals more or less accurately identify the direction of the food source (e.g. by smelling) and move towards maxima of F. We therefore consider the unit vector that describes the orientation of the field to be given by

$$\gamma(x) = \frac{\nabla F(x)}{\|\nabla F(x)\|}.$$

Since orientation of individuals is rarely perfect (i.e. movement will not be directly in the direction of the food) we take a (unimodal) von Mises distribution about the gradient of F:

$$\tilde{q}(x,\theta) = \frac{1}{2\pi I_0(k)} e^{k\theta\cdot\gamma}. \tag{56}$$

The above defines a direction distribution in which individuals align and migrate in the direction of the source. Note that varying degree of alignment could also be incorporated, for example through allowing k to depend on the size of F or $\|\nabla F(x)\|$. To determine the macroscopic terms we again compute the moments of the distribution (see Appendix):

$$\mathbb{E}_q(x) = \frac{I_1(k)}{I_0(k)}\gamma; \tag{57}$$

$$\mathbb{V}_q = \frac{1}{2}\left(1 - \frac{I_2(k)}{I_0(k)}\right)\mathbb{I}_2 + \left(\frac{I_2(k)}{I_0(k)} - \left(\frac{I_1(k)}{I_0(k)}\right)^2\right)\gamma\gamma^T. \tag{58}$$

Notably, the drift term $\mathbb{E}_q$ is now nonzero and in the direction of $\nabla F(x)$, whereas the diffusion term has two components: an isotropic part and an oriented nonisotropic part, which is proportional to $\nabla F(x)\nabla F(x)^T$. The resulting macroscopic equation is therefore of the form of an anisotropic drift-diffusion equation

$$p_t + s\nabla(\mathbb{E}_q p) = \frac{s^2}{\mu}\nabla(\nabla\mathbb{V}_q p). \tag{59}$$

It is worth noting two limiting scenarios. For the parameter of concentration k becoming small (i.e. the food source provides a weak orientational cue), then

$$\lim_{k\to 0}\mathbb{E}_q = 0 \qquad \lim_{k\to 0}\mathbb{V}_q = \frac{1}{2}\mathbb{I}_2,$$

and we obtain uniform isotropic diffusion and no accumulation at the food source. For the parameter of concentration k becoming large (i.e. the food source provides a strong orientational cue), then

$$\lim_{k\to\infty} \mathbb{E}_q = \gamma \qquad \lim_{k\to\infty} \mathbb{V}_q = 0\,,$$

and hence we obtain the pure drift equation in which cells move directly towards the food source with speed s.

7.2.1 Anisotropic diffusion-drift example

To illustrate how unidirectional environments impact on patterning, we present a scenario analogous to the example of (7.1.2). Specifically, we consider a population in a landscape with a unidirectional patch in the centre of the domain. We assume the above von Mises distribution (56) with the main orientation along the diagonal $\gamma = (1/\sqrt{2}, 1/\sqrt{2})^T$,

$$q(x,\theta) = \frac{1}{2\pi I_0(k)} e^{k(x)\theta\cdot\gamma}\,.$$

Once again $k(x)$ is assumed to decay exponentially from the centre to the periphery of the domain, with

$$k(x) = k_0 e^{-r|x|^2}\,.$$

Here we set $k_0 = 5$ and $r = 1.0$.

We again perform a direct simulation of the original transport model (3) with the above choice for q and solving subject to the same initial and boundary conditions as for the example of Section 7.1.2. As we observe in Figure 4E, the directed patch significantly impacts on the subsequent distribution of the population. Rapid transportation through the oriented region results in a markedly decreased population density within this region. This generates a large "plume"-like structure adjacent to this region.

We simulate the corresponding anisotropic diffusion-drift equation. For the above von Mises distribution we compute the heterogeneous drift and diffusion terms from (57) and (58) respectively and substitute these into (59). Simulations show an excellent quantitative match with the transport model, Figure 4F, once again confirming the validity of the macroscopic scaling process.

7.2.2 Relation to haptotaxis and chemotaxis

As a brief remark we note that unidirectional environments can be reinterpreted in terms of modelling haptotaxis (directed migration of cells in response to regions of high adhesivity in the ECM), chemotaxis (directed movement in response to chemical gradients) and other forms of gradient following. Haptotaxis and chemotaxis are typically modelled by an advective type term in PDE models (e.g. see

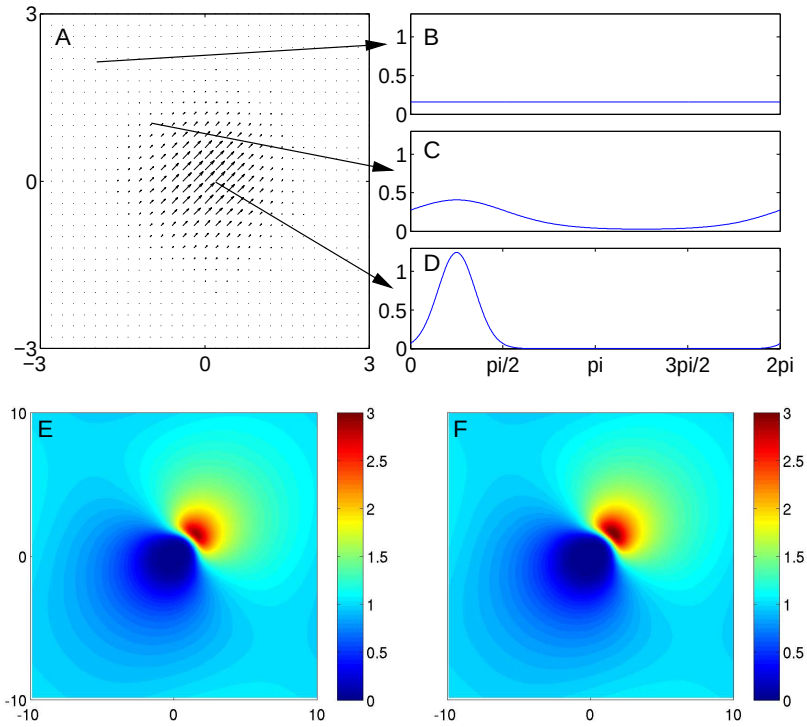

Fig. 4 Population heterogeneity arising due to unidirectional orientation of the environment. (A)-(D) representation of the imposed anisotropy, with (A) representing strength of anisotropy k (length of line segments) and the directional alignment of the field (figure truncated at ± 3 to aid clarity of presentation) and (B)-(D) plotting the corresponding distribution (56) at each point indicated, plotted as a function of $\theta = (\cos\phi, \sin\phi)$ for $\phi \in [0, 2\pi)$. Note that the dominating orientation corresponds to $\gamma = (\sqrt{2}/2, \sqrt{2}/2)$. (E) Simulation of the transport model (3) under the imposed q, showing the predicted macroscopic cell density $\bar{p}$ at time $t = 50$ for $s = 10$ and $\mu = 100$. (F) Simulation of the diffusion-drift limit (59), using $s = 10$ and $s^2/\mu = 1$ and plotted at $t = 50$, with the diffusion tensor computed from (58) and the drift term calculated according to (57). For details of the numerical implementation we refer to the Appendix.

[24, 20, 33, 29, 2]), with cell velocity proportional to the adhesion/chemical gradient.

The present work provides new motivation for such models. For example, we assume $F(x)$ describes the ECM adhesivity field surrounding a cell and take the von Mises distribution (56) to describe oriented movement towards higher adhesion, i.e. we take q to be given by

$$q(x,v) = \delta_{s(\|\nabla F\|)}(\|v\|)\frac{1}{2\pi I_0(k)}\exp\left(k\frac{v\cdot\nabla F(x)}{\|v\|\,\|\nabla F(x)\|}\right).$$

Furthermore, we let the speed s depend on the strength of the gradient, $s(\|\nabla F(x)\|)$. Since $\mathbb{E}_q \neq 0$, the parabolic limit does not apply and we employ instead the hyperbolic scaling. Drift subsequently dominates with diffusion of lower order and the corresponding macroscopic model becomes (to leading order)

$$u_t + 2\pi I_1(k)\nabla \cdot \left(\frac{s(\|\nabla F\|)}{\|\nabla F\|} \nabla F u \right) = 0.$$

The field F could also be reinterpreted to describe other forms of tactic migration.

7.3 Singular distributions

The theories above have been derived for regular measures $q \in L^2$ only and, while it is possible to extend some of the results to singular measures (see for example [18, 7]), the mathematical overhead becomes enormous; here we simply apply the formal limit equations in good faith. Singular measures, however can play an important role either in describing certain oriented fields or representing a limit scenario for previously considered cases.

7.3.1 Strictly bidirectional: degenerate diffusion

If we consider the earlier bimodal von Mises distribution (49) and let $k \to \infty$ we converge to two point measures in directions γ and $-\gamma$. Such distributions could be considered as completely aligned and bidirectional networks. Specifically, we let

$$q(x) := \frac{1}{2}(\delta_{\gamma(x)}(v) + \delta_{-\gamma(x)}(v)),$$

and find

$$\mathbb{E}_q = 0 \quad \text{and} \quad \mathbb{V}_q = \gamma\gamma^T. \tag{60}$$

Thus, there is zero drift and diffusion is given by a rank-one tensor $\mathbb{V}_q$, i.e. diffusion occurs only along the $\gamma/-\gamma$ axis. The corresponding diffusion tensor $D = \frac{s^2}{\mu}\mathbb{V}_q$ is degenerate and not elliptic, hence the general solution theory for parabolic equations does not apply. In a forthcoming paper we develop methods that allows us to describe *very weak* solutions for such degenerate problems [21].

7.3.2 Strictly Unidirectional: Relation to ODEs

For the corresponding unimodal von Mises distribution (56) with $k \to \infty$ we obtain a singular distribution. This defines a strictly aligned unidirectional field and, as

described in [17], there is a striking relation between these limit equations and the theory of ordinary differential equations (ODE).

The solution of the autonomous differential equation

$$\dot{x}(t) = f(x(t)) \tag{61}$$

in the domain $\mathbb{R}^n$ is given by the solution semigroup $\Phi(t, x_0)$ which describes orbits that are tangential to the vector field $f(x)$. In our notation here, we assume that this vector field $f(x) \in V$ defines a given direction at each point in $\mathbb{R}^n$ and define

$$q(x, v) = \delta_{f(x)}(v), \tag{62}$$

where δ_f denotes the point measure with mass in $f \in V$. In this case we find

$$\mathbb{E}_q(x) = f(x), \quad \text{and} \quad \mathbb{V}_q = 0.$$

This is a clearly drift-dominated situation and the hyperbolic scaling is appropriate. Item 4. of Lemma 1 applies and we obtain the limit equation

$$u_t + \nabla(f(x)u) = 0.$$

This hyperbolic PDE has the characteristics

$$\dot{x}(t) = f(x(t)),$$

which is the ODE from above. Hence typical movement paths of particles in an environment given by a singular measure (62) are orbits of the corresponding ODE.

7.4 Life in a stream

An example that amalgamates various cases above (nondirectional, unidirectional and singular) is the movement of living organisms in a stream (which, for convenience, is assumed to be two dimensional).

Movement can be split into two principal contributions: (i) transport due to the current, and (ii) active movement by the individuals. For transport due to the current we let $\gamma(x)$ denote the direction of the stream (assumed quasi-constant over the timescale of interest), and let $q_1(\theta) = \delta_{\gamma(x)}(\theta)$ define the stream current. We augment this transport with a degree of turbulence, expressed via the random movement contribution $q_2(\theta) = |\mathbb{S}^{n-1}|^{-1}$.

For the active movement we assume individuals are biased towards a given food source

$$q_3(\theta) = \frac{1}{2\pi I_0(k)} e^{k\theta \cdot \Gamma(x)}, \quad \text{with} \quad \Gamma(x) = \frac{\nabla F(x)}{\|\nabla F(x)\|},$$

where $F(x)$ describes the distribution of food inside the stream. To simplify computations, we assume individuals have a preferred speed s, i.e. $V = s\mathbb{S}^{n-1}$. Hence, q is a convex combination of the above effects:

$$q(x,v) = s^{1-n}\left(\alpha_1 q_1(\hat{v}) + \alpha_2 q_2(\hat{v}) + \alpha_3 q_3(\hat{v})\right),$$

where $\alpha_1 + \alpha_2 + \alpha_3 = 1$, and $\alpha_i \geq 0$ for $i = 1, ..., 3.$, and $\hat{v} = v/\|v\|$ denotes the unit vector in direction of v.

In this case, the macroscopic drift component is given by

$$\mathbb{E}_q = \alpha_1 \gamma(x) + s\alpha_3 2\pi I_1(k)\Gamma(x).$$

Drift arises as the interplay between transport due to the stream $\gamma(x)$ and movement towards the food source $\Gamma(x)$. The diffusion term is given by

$$D(x) = \frac{s^2}{\mu}\left[\frac{\alpha_2}{2}\mathbb{I}_2 + \frac{\alpha_3}{2}\left(1 - \frac{I_2(k)}{I_0(k)}\right)\mathbb{I}_2 + \alpha_3\left(\frac{I_2(k)}{I_0(k)} - \left(\frac{I_1(k)}{I_0(k)}\right)^2\right)\Gamma(x)\Gamma(x)^T\right],$$

derived from a combination of random movement and the imperfect response to the food source. We note that more detailed modelling of river ecosystems and species survival has been undertaken by Lutscher, et al. [28].

8 Conclusion and Discussion

The principal aims of this paper have been to demonstrate the effectiveness of transport equations as a method for modelling cell or animal movement, to explain and summarise the various scaling limits that allow their approximation to distinct macroscopic models, and to consider a few pertinent ecological applications, such as wolf movement on seismic lines, attraction to a food source and movement in rivers.

The transport model is a natural model for movement, relying as it does on experimentally measurable data such as speeds and turning rates for its key inputs. While it is certainly possible to study the transport model directly, both the analytical and numerical overheads can be costly. For example, the numerical solution of the simple (and assumed 2D) transport model given by (3) requires discretisation not only over space, but also orientation; extensions to relevant scenarios such as 3D, variable speeds or more intricate turning functions would significantly add to the computational time. Simplifying to the relatively straightforward macroscopic model, which still possesses details of the underlying microscopic processes in its macroscopic parameters, allows far faster numerical computation while opening the vault to a wealth of analytical tools.

Typically the scaling methods considered here (parabolic scaling, hyperbolic scaling, and moment closure) are studied separately and it can be difficult for unfamiliar readers to determine why one method is chosen over another. By focussing

on a specific formulation of a transport model, originally developed to describe cell movement in network tissues, we could transparently derive the various limiting equations and expose the assumptions that underlie them.

Responding to a question posed during the introduction, it would be bold to categorically state a "best" method and instead models must be treated on a case by case basis. Succinctly, it comes down to the relative size of drift and diffusion terms: when the model is drift-dominated, as occurs for environments with a strong cue in a specific direction, the hyperbolic approximation applies; when the model is diffusion-dominated, as for environments with either nondirectional or bidirectional orientation, the parabolic limit is appropriate; if the two effects are of a similar order then either the moment closure or the hyperbolic model with corrections provide the most appropriate approximation.

It is worth noting that the clarity of the analysis here is a direct product of the simplicity of our transport model. Full analyses for more general kinetic equations can become highly technical and fill entire textbooks (for example, see [8] for diluted gases or [39, 5] for biological applications). With the aim of illuminating the various scaling limits we have made a number of convenient assumptions and it is worth describing some of the limiting factors here, and their potential importance for biological applications.

- We have not considered time-varying habitats. In many instances, the environment can change considerably on the timescale of movement, either independently (for example, the changing position of the sun or alterations in wind strength) or through direct modification by the migrating population (e.g. formation of pheromone trails by ants or restructuring the ECM by cells). The addition of t-dependence in the orientation function q adds a significant level of complexity and, while the scaling limits do apply, they require detailed analysis and consideration on a case by case basis. For details of such analyses in the context of mesenchymal cell migration we refer to [17].
- In this paper, the environment has been assumed to only impact on the turning of individuals, not on their speed. While it is trivial to extend the original transport model to incorporate more general speed dependencies, the subsequent computations to calculate the scaling limits are often complex and obscure their basic features. We note that in the context of taxes above, we have given one simple example on how to perform scaling for nonconstant speeds. The one-dimensional case has been studied in detail in [23, 22]
- Appropriate boundary conditions on bounded domains require special attention. For example in the case of the seismic lines above, what would be meaningful boundary conditions on and off the seismic lines for both the original transport model and the subsequent macroscopic limits? We circumnavigated this issue in the simulations by buffering the simulated region with a surrounding isotropic region and using periodic boundary conditions, however other conditions could certainly be considered. For example, zero-flux boundary conditions could be one relevent choice, as assumed in [31].
- More complicated formulations for the turning kernel $T(x,v,v')$ and non-constant turning rates $\mu(t,x,p,v)$ arise naturally in many applications. Obviously, any

such choice should be tailored according to the application under analysis, however the ensuing calculations can become highly intricate. One important yet complicated case is the incorporation of interactions between individuals. For example, the patterns formed by many migrating populations, from bird flocks to wildebeest, are highly structured through the response of an individual to the movement of a neighbour.

- The simple model here has neglected aspects such as a resting phase (individuals are assumed to move continuously) or population kinetics. For example, modelling the impact of seismic lines on the predator-prey dynamics of wolves and caribou would require an extension of the model to include a separate caribou population and appropriate predator-prey interactions. Again, while tailoring the original transport model to include such extensions is relatively straightforward, the subsequent calculation of scaling limits would require treatment on a case by case basis.
- On a technical side, in our theorems we have typically used the notion"is approximated by" to denote the formal limit considerations. Rigorously, to refer to an approximation property would require proof of convergence in an appropriate function space and we have completely omitted these issues here. Rigorous convergence results for the parabolic limit can be found in [19, 9].

Migration, whether cellular or animal, clearly is immensely relevant to a plethora of crucial biological and ecological processes. Distinct methods offer different advantages, allowing multiple windows through which the underlying mechanisms can be observed. In this paper, our aim has been to concentrate on the transport (and associated macroscopic) equations, with the key aim of shedding illumination on this useful modelling approach.

Appendix

9 Moments of von Mises distributions

The appendix is used to present an alternative method for computing moments of a von Mises distribution. Usually, moments are computed through explicit trigonometric integrations (see e.g. [30], [32], [3]) however here we instead apply the divergence theorem. While this method is easily generalised to arbitrary space dimensions, explicit trigonometric integration becomes increasingly cumbersome with increases in the space dimension.

Given a unit vector $\gamma \in \mathbb{S}^{n-1}$, we first study the (unimodal) von Mises distribution

$$q(\theta) = \frac{1}{2\pi I_0(k)} e^{k\theta\cdot\gamma} \tag{63}$$

In the main text it is noted that the moments employ Bessel functions and we begin by collecting a few of their properties. If $J_n(x)$ denote the Bessel functions of

first kind, then

$$I_n(x) := (-i)^{-n} J_n(ix)$$

denotes the Bessel function of first kind with purely imaginary argument, or the *modified Bessel functions*. For these we have the relation

$$I_n(k) = \frac{1}{2\pi} \int_0^{2\pi} \cos(n\phi) e^{k\cos\phi} d\phi \,. \tag{64}$$

Two further important relations include the differential recurrence

$$\frac{d}{dx}\left(x^n J_n(x)\right) = x^n J_{n-1}(x) \tag{65}$$

for $n \geq 0$, and the recurrence relation

$$J_{n+1}(x) = \frac{2n}{x} J_n(x) - J_{n-1}(x). \tag{66}$$

9.1 Unimodal von Mises distribution

To compute the total mass of the (unimodal) von Mises distribution (63) we denote the angle between θ and γ by ϕ:

$$\int_{\mathbb{S}^1} q(\theta) d\theta = \frac{1}{2\pi I_0(k)} \int_0^{2\pi} e^{k\cos\phi} d\phi = 1,$$

where we used (64).

To compute the expectation, we note

$$\begin{aligned}
2\pi I_0(k)\mathbb{E}_q &= \int_{\mathbb{S}^1} \theta e^{k\theta\cdot\gamma}, \\
&= \int_{\mathbb{B}_1(0)} \mathrm{div}_v \, e^{kv\cdot\gamma} dv, \\
&= \int_{\mathbb{B}_1(0)} k\gamma e^{kv\cdot\gamma} dv, \\
&= k\gamma \int_0^1 \int_0^{2\pi} e^{rk\cos\phi} r dr d\phi \,, \\
&= k\gamma \int_0^1 2\pi r I_0(rk) dr, \\
&= 2\pi k\gamma \int_0^1 r I_0(rk) dr \,.
\end{aligned}$$

To solve the last integral, we use (65) and write

$$rI_0(rk) = \frac{irkJ_0(irk)}{ik} = \frac{1}{ik}\frac{d}{dx}(xJ_1(x))|_{x=irk} = \frac{1}{ik}\frac{d}{dr}(rJ_1(irk)).$$

Then

$$\int_0^1 rI_0(rk)dr = \frac{1}{ik}rJ_1(ik) = \frac{1}{ik}iI_1(k) = \frac{I_1(k)}{k}. \tag{67}$$

and we find

$$\mathbb{E}_q = \frac{I_1(k)}{I_0(k)}\,\gamma. \tag{68}$$

The variance-covariance matrix is given by

$$\mathbb{V}_q = \int_{\mathbb{S}^1}(\theta - \mathbb{E}_q)(v - \mathbb{E}_q)^T q(\theta)d\theta = \int_{\mathbb{S}^1}\theta\theta^T q(\theta)d\theta - \mathbb{E}_q\mathbb{E}_q^T.$$

To find the second moment of q we consider two test vectors $a, b \in \mathbb{R}^2$ and employ index notation for automatic summation over repeated indices

$$\begin{aligned}
2\pi I_0(k)a\int_{\mathbb{S}^1}\theta\theta^T q(\theta)d\theta\, b &= \int_{\mathbb{S}^1} a_i\theta^i b_j\theta^j e^{k\theta^l\gamma_l}d\theta \\
&= \int_{\mathbb{S}^1}\theta^i(a_i b_j\theta^j e^{k\theta^l\gamma_l})d\theta \\
&= \int_{\mathbb{B}_1(0)}\frac{\partial}{\partial v^i}(a_i b_j v^j e^{kv^l\gamma_l})dv \\
&= \int_{\mathbb{B}_1(0)} a_i b_i e^{kv\cdot\gamma}dv + \int_{\mathbb{B}_1(0)} a_i(v\cdot b)k\gamma_i e^{kv\cdot\gamma}dv \\
&= a\cdot b\int_{\mathbb{B}_1(0)} e^{kv\cdot\gamma}dv + ka\cdot\gamma\, b\cdot\int_{\mathbb{B}_1(0)} ve^{kv\cdot\gamma}dv
\end{aligned} \tag{69}$$

The first integral in (69) can be solved directly

$$\int_{\mathbb{B}_1(0)} e^{kv\cdot\gamma}dv = \int_0^1\int_{\mathbb{S}^1} e^{rk\theta\cdot\gamma}rdrd\theta = \int_0^1 2\pi rI_0(rk)dr = 2\pi\frac{I_1(k)}{k},$$

where we used (64) and (67) in the penultimate and ultimate step respectively. Using (64) we can transform the second integral from (69) as follows:

$$\begin{aligned}
\int_{\mathbb{B}_1(0)} ve^{kv\cdot\gamma}dv &= \int_0^1\int_{\mathbb{S}^1} r\theta e^{rk\theta\cdot\gamma}rdrd\theta = \int_0^1 r^2\int_{\mathbb{S}^1}\theta e^{rk\theta\cdot\gamma}d\theta \\
&= 2\pi\gamma\int_0^1 r^2 I_1(rk)dr,
\end{aligned} \tag{70}$$

where we used (68) in the last step.

Now we use the differential recurrence relation (65) to write

$$r^2 I_1(rk) = -\frac{1}{ik^2}(irk)^2 J_1(irk) = -\frac{1}{ik^2}\frac{d}{dx}(x^2 J_1(x))|_{x=irk} = -\frac{1}{k}\frac{d}{dr}(r^2 J_1(irk)).$$

Continuing from (70) we find

$$\int_{\mathbb{B}_1(0)} ve^{kv\cdot\gamma}dv = -2\pi\gamma\int_0^1 \frac{1}{k}\frac{d}{dr}(r^2 J_1(irk))dr = -2\pi\gamma J_2(ik) = 2\pi\gamma\frac{I_2(k)}{k}. \quad (71)$$

Substituting all the integrals back into equation (69)

$$\begin{aligned} a\int_{\mathbb{S}^1}\theta\theta^T q(\theta)d\theta\, b &= a\cdot b\frac{2\pi\frac{I_1(k)}{k}}{2\pi I_0(k)} + ka\cdot\gamma\frac{2\pi\gamma\cdot b\frac{I_2(k)}{k}}{2\pi I_0(k)} \\ &= a\left(\frac{1}{k}\frac{I_1(k)}{I_0(k)}\mathbb{I}_2 + \gamma\gamma^T\frac{I_2(k)}{I_0(k)}\right)b. \end{aligned}$$

Finally, we use the identity (66) for $n=1$ to replace

$$\frac{1}{k}\frac{I_1(k)}{I_0(k)} = \frac{1}{2}\left(1-\frac{I_2(k)}{I_0(k)}\right)$$

and the second moment is given by

$$\int_{\mathbb{S}^1}\theta\theta^T q(\theta)d\theta = \frac{1}{2}\mathbb{I}_2 + \frac{I_2(k)}{I_0(k)}\left(\gamma\gamma^T - \frac{1}{2}\mathbb{I}_2\right). \quad (72)$$

Together with the formula for the expectation (68) we find

$$\begin{aligned} \mathbb{V}_q &= \int_{\mathbb{S}^1}\theta\theta^T q(\theta)d\theta - \mathbb{E}_q\mathbb{E}_q^T \\ &= \frac{1}{2}\mathbb{I}_2 + \frac{I_2(k)}{I_0(k)}\left(\gamma\gamma^T - \frac{1}{2}\mathbb{I}_2\right) - \left(\frac{I_1(k)}{I_0(k)}\right)^2\gamma\gamma^T \quad (73) \\ &= \frac{1}{2}\left(1-\frac{I_2(k)}{I_0(k)}\right)\mathbb{I}_2 + \left(\frac{I_2(k)}{I_0(k)} - \left(\frac{I_1(k)}{I_0(k)}\right)^2\right)\gamma\gamma^T. \quad (74) \end{aligned}$$

Clearly, if the parameter of concentration k becomes small (i.e. $k\to 0$) then $\mathbb{E}_q\to 0$ and $\mathbb{V}_q\to\frac{1}{2}\mathbb{I}_2$.

9.2 Bimodal von Mises distribution

Computations for the bimodal von Mises distribution

$$q(\theta) = \frac{1}{4\pi I_0(k)}\left(e^{k\theta\cdot\gamma} + e^{-k\theta\cdot\gamma}\right)$$

are very similar. Since the bimodal von Mises distribution is symmetric (or undirected) we have $\mathbb{E}_q = 0$ and $\mathbb{V}_q = \int\theta\theta^T q(\theta)d\theta$. We apply formula (72) for each of the components $e^{k\theta\cdot\gamma}$ and $e^{-k\theta\cdot\gamma}$ separately and sum. We find

$$\mathbb{V}_q = \frac{1}{2}\left(1 - \frac{I_2(k)}{I_0(k)}\right)\mathbb{I}_2 + \frac{I_2(k)}{I_0(k)}\gamma\gamma^T.$$

10 Numerical methods

10.1 Simulations of transport model

Simulations of the transport model (3) were performed with a Method of Lines (MOL) approach, in which space and velocity are discretised into a high-dimensional system of time-dependent ODEs (the MOL-ODEs). For the transport equations presented, the rectangular spatial domain (of dimensions $L_x \times L_y$) was discretised into a uniform mesh of 201 by 201 points, while velocity $v = s(\cos\alpha, \sin\alpha)$ (for $\alpha \in [0, 2\pi)$) was discretised into 100 uniformly spaced orientations with a fixed speed s. Spatial terms for particle movement were approximated in conservative form using a third-order upwinding scheme, augmented by flux-limiting to maintain positivity. The resulting MOL-ODEs were integrated in time using the ROWMAP stiff systems integrator [42], with a fixed absolute and relative error tolerance of 10^{-7}. Similar approaches to those above were employed in [36].

10.2 Simulations of macroscopic models

Simulations of both the anisotropic diffusion (51) and anisotropic drift-diffusion (59) model were performed with a similar MOL approach. The anisotropic diffusion term was factored into diffusive and convective terms and solved in conservative form, applying a central difference scheme for the former and first order upwinding for the latter. The additional drift terms in the drift-diffusion model were also solved with first order upwinding and the resulting MOL-ODEs were integrated in time using ROWMAP with error tolerances of 10^{-7}. For the two simulations in Figures 2 and 4 we used 201 by 201 mesh points for the spatial discretisation, while for the simulations in Figure 3 we use 500 by 500 mesh points. We note that simulations with finer spatial discretisations and smaller tolerances demonstrated no appreciable quantitative difference.

References

1. W. Alt. Biased random walk model for chemotaxis and related diffusion approximation. *J. Math. Biology*, 9:147–177, 1980.
2. A.R.A. Anderson, M.A.J. Chaplain, E.L. Newman, R.J.C. Steele, and A.M. Thompson. Mathematical modelling of tumour invasion and metastasis. *J. theor. Med.*, 2:129–154, 2000.
3. E. Batschelet. *Circular Statistics in Biology*. Academic Press, London, 1981.

4. N. Bellomo. *Modeling complex living systems - Kinetic theory and stochastic game approach*. Birkhauser, 2008.
5. N. Bellomo and M.L. Schiavo. *Lecture Notes on the Mathematical Theory of Generalized Boltzmann Methods*. World Scientific, Singapore, 2000.
6. G. P. Brown, B. L. Phillips, J. K. Webb, and R. Shine. Toad on the road: Use of roads as dispersal corridors by cane toads (bufo marinus) at an invasion front in tropical australia. *Biol. Cons.*, 133(1):88–94, 2006.
7. J.A. Carrillo, R.M. Colombo, P. Gwiazda, and A. Ulikowska. Structured populations, cell growth and measure valued balance laws. 2011. Preprint UAB.
8. C. Cercignani, R. Illner, and M. Pulvirenti. *The Mathematical Theory of Diluted Gases*. Springer, New York, 1994.
9. F.A.C.C. Chalub, P.A. Markovich, B. Perthame, and C. Schmeiser. Kinetic models for chemotaxis and their drift-diffusion limits. *Monatsh. Math.*, 142:123–141, 2004.
10. A. Chauviere, T. Hillen, and L. Preziosi. Modeling cell movement in anisotropic and heterogeneous network tissues. *Networks and Heterogeneous Media*, 2:333–357, 2007.
11. Y. Dolak and C. Schmeiser. Kinetic models for chemotaxis: Hydrodynamic limits and spatio-temporal mechanics. *J. Math. Biol.*, 51:595–615, 2005.
12. G. A. Dunn and J. P. Heath. A new hypothesis of contact guidance in tissue cells. *Exp. Cell Res.*, 101:1–14, 1976.
13. P. Friedl and E.B. Bröcker. The biology of cell locomotion within three dimensional extracellular matrix. *Cell Motility Life Sci.*, 57:41–64, 2000.
14. P. Friedl and K. Wolf. Tumour-cell invasion and migration: diversity and escape mechanisms. *Nature Rev.*, 3:362–374, 2003.
15. S. Guido and R. T. Tranquillo. A methodology for the systematic and quantitative study of cell contact guidance in oriented collagen gels. Correlation of fibroblast orientation and gel birefringence. *J. Cell. Sci.*, 105:317–331, 1993.
16. T. Hillen. On the L^2-closure of transport equations: The general case. *Discrete and Cont. Dyn. Syst. Series B*, 5(2):299–318, 2005.
17. T. Hillen. M^5 mesoscopic and macroscopic models for mesenchymal motion. *J. Math. Biol.*, 53(4):585–616, 2006.
18. T. Hillen, P. Hinow, and Z.A. Wang. Mathematical analysis of a kinetic model for cell movement in network tissues. *Discrete and Continuous Dyn. Syst. - B*, 14(3):1055–1080, 2010.
19. T. Hillen and H.G. Othmer. The diffusion limit of transport equations derived from velocity jump processes. *SIAM J. Appl. Math.*, 61(3):751–775, 2000.
20. T. Hillen and K.J. Painter. A user's guide to PDE models for chemotaxis. *J. Math. Biol.*, 58:183–217, 2009.
21. T. Hillen, K.J. Painter, and M. Winkler. Anisotropic diffusion can lead to singularity formation. 2012. In preparation.
22. T. Hillen, C. Rohde, and F. Lutscher. Existence of weak solutions for a hyperbolic model for chemosensitive movement. 2001. to appear in J. Math. Ana. Appl.
23. T. Hillen and A. Stevens. Hyperbolic models for chemotaxis in 1-d. *Nonlinear Analysis: Real World Applications*, 1(1):409–433, 2001.
24. E.F. Keller and L.A. Segel. Initiation of slime mold aggregation viewed as an instability. *J. theo. Biology*, 26:399–415, 1970.
25. M. Lachowicz. Microscopic, mesoscopic and macroscopic descriptions of complex systems. *Prob. Engin. Mech.*, 26:54–60, 2011.
26. H. P. Lipp, A. L. Vyssotski, D. P. Wolfer, S. Renaudineau, M. Savini, G. Troster, and G. Dell'Omo. Pigeon homing along highways and exits. *Curr. Biol.*, 14(14):1239–1249, 2004.
27. K. J. Lohmann, C. M. Lohmann, and C. S. Endres. The sensory ecology of ocean navigation. *J. Exp. Biol.*, 211:1719–1728, 2008.
28. F. Lustcher, E. Pachepsky, and M.A. Lewis. The effect of dispersal patterns on stream populations. *SIAM Rev.*, 478:749–7725, 2005.
29. P.K. Maini. Spatial and spatio-temporal patterns in a cell-haptotaxis model. *J. Math. Biol.*, 27:507–522, 1989.

30. H.W. McKenzie. Linear features impact predator-prey encounters: analysis and first passage time, 2006. MSc thesis, University of Alberta.
31. H.W. McKenzie, E.H. Merrill, R.J. Spiteri, and M.A. Lewis. How linear features alter predator movement and the functional response. 2011. submitted.
32. P. Moorcroft and M.A. Lewis. *Mechanistic Home Range Analysis*. Princeton University Press, Princeton, 2006.
33. G. Oster, J.D. Murray, and A. Harris. Mechanical aspects of mesenchymal morphogenesis. *J. Embryol. Exp. Morphol.*, 78:83–125, 1983.
34. H.G. Othmer, S.R. Dunbar, and W. Alt. Models of dispersal in biological systems. *J. Math. Biol.*, 26:263–298, 1988.
35. H.G. Othmer and A. Stevens. Aggregation, blowup and collapse: The ABC's of taxis in reinforced random walks. *SIAM J. Appl. Math.*, 57:1044–1081, 1997.
36. K.J. Painter. Modelling migration strategies in the extracellular matrix. *J. Math. Biol.*, 58:511–543, 2009.
37. K.J. Painter, T. Hillen, and J.E. Chimal Eguia. Connecting DTI data to anisotropic diffusion models for glioma growth. 2012. In preparation.
38. G. Pe'er, D. Saltz, H. Thulke, and U. Motro. Response to topography in a hilltopping butterfly and implications for modelling nonrandom dispersal. *Animal Behaviour*, 68:825–839, 2004.
39. B. Perthame. *Transport Equations in Biology*. Birkhäuser, 2007.
40. A. M. Reynolds, T. K. Dutta, R. H. Curtis, S. J. Powers, H. S. Gaur, and B. R. Kerry. Chemotaxis can take plant-parasitic nematodes to the source of a chemo-attractant via the shortest possible routes. *J R Soc Interface*, 8:568–577, 2011.
41. S. M. Tomkiewicz, M. R. Fuller, J. G. Kie, and K. K. Bates. Global positioning system and associated technologies in animal behaviour and ecological research. *Phil. Trans. R. Soc. B*, 365:21632176, 2010.
42. R. Weiner, B.A. Schmitt, and Podhaisky H. Rowmap–a row-code with Krylov techniques for large stiff ODEs. *Appl. Num. Math.*, 25:303–319, 1997.
43. P. C. Wilkinson and J. M. Lackie. The influence of contact guidance on chemotaxis of human neutrophil leukocytes. *Exp. Cell Res.*, 145:255–264, 1983.
44. K. Wolf, R. Muller, S. Borgmann, E. B. Brocker, and P. Friedl. Amoeboid shape change and contact guidance: T-lymphocyte crawling through fibrillar collagen is independent of matrix remodeling by MMPs and other proteases. *Blood*, 102:3262–3269, 2003.
45. A. Wood and P. Thorogood. An analysis of in vivo cell migration during teleost fin morphogenesis. *J. Cell Sci.*, 66:205–222, 1984.